Communication-Sensing Region for Cell-Free Massive MIMO ISAC Systems

Weihao Mao, *Student Member, IEEE*, Yang Lu, *Member, IEEE*, Chong-Yung Chi, *Life Fellow, IEEE*, Bo Ai, *Fellow, IEEE*, Zhangdui Zhong, *Fellow, IEEE*, and Zhiguo Ding, *Fellow, IEEE*

***Abstract*— This paper investigates the system model and the transmit beamforming design for the Cell-Free massive multi-input multi-output (MIMO) integrated sensing and communication (ISAC) system. The impact of the uncertainty of the target locations on the propagation of wireless signals is considered during both uplink and downlink phases, and especially, the main statistics of the MIMO channel estimation error are theoretically derived in the closed-form fashion. A fundamental performance metric, termed communication-sensing (C-S) region, is defined for the considered system via three cases, i.e., the sensing-only case, the communication-only case and the ISAC case. The transmit beamforming design problems for the three cases are respectively carried out through different reformulations, e.g., the Lagrangian dual transform and the quadratic fractional transform, and some combinations of the block coordinate descent method and the successive convex approximation method. Numerical results present a 3-dimensional C-S region with a dynamic number of access points to illustrate the trade-off between communication and radar sensing. The advantage for radar sensing of the Cell-Free massive MIMO system is also studied via a comparison with the traditional cellular system. Finally, the efficacy of the proposed beamforming schemes is validated in comparison with zero-forcing and maximum ratio transmission schemes.**

***Index Terms*— ISAC, cell-free massive MIMO, C-S region, beamforming.**

Manuscript received 15 June 2023; revised 20 January 2024 and 24 March 2024; accepted 15 April 2024. Date of publication 30 April 2024; date of current version 12 September 2024. This work was supported in part by Beijing Nova Program under Grant Z211100002121139, in part by China Postdoctoral Science Foundation under Grant BX2021031 and Grant 2021M690342, and in part by the National Natural Science Foundation of China (NSFC) under Grant 62101025 and Grant 62221001. The work of Chong-Yung Chi was supported by the National Science and Technology Council (NSTC) under Grant NSTC 111-2221-E-007-035-MY2. The associate editor coordinating the review of this article and approving it for publication was Y. Zhang. *(Corresponding author: Yang Lu.)*

Weihao Mao and Yang Lu are with the School of Computer Science and Technology, Beijing Jiaotong University, Beijing 100044, China (e-mail: weihaomao@bjtu.edu.cn; yanglu@bjtu.edu.cn).

Chong-Yung Chi is with the Institute of Communications Engineering, Department of Electrical Engineering, National Tsing Hua University, Hsinchu 30013, Taiwan (e-mail: cychi@ee.nthu.edu.tw).

Bo Ai and Zhangdui Zhong are with the School of Electronics and Information Engineering, Beijing Jiaotong University, Beijing 100044, China (e-mail: boai@bjtu.edu.cn; zhdzhong@bjtu.edu.cn).

Zhiguo Ding is with the Department of Electrical Engineering and Computer Science, Khalifa University, Abu Dhabi, United Arab Emirates (e-mail: zhiguo.ding@ieee.org).

Color versions of one or more figures in this article are available at https://doi.org/10.1109/TWC.2024.3392330.

Digital Object Identifier 10.1109/TWC.2024.3392330

I. Introduction

A. Background

With the development of mobile intelligent applications, e.g., auto-driving and indoor location, sensing has played a more important role than ever before [1]. Besides, there has been a huge increment in the number of smart devices and the future 6G networks have come up with higher requirements for the communication rates [2], [3], [4]. The above facts motivate the joint design of communication and sensing. Integrated sensing and communication (ISAC) is an emerging technique which utilizes the same spectrum resource to realize both communication and radar sensing functions [5]. In the literature, there are two ISAC architectures. One is the coexisting radar and communication (CRC) architecture, where the radar and the communication base station (BS) are located separately, and the sensing beam and the communication beam are also generated individually [6]. The other is the dual functional radar-communication (DFRC) architecture, where the radar and the communication BS are co-located, i.e., they are integrated as an ISAC BS with shared hardwares [7]. Therefore, the sensing beam and the communication beam can be jointly generated. Compared with the CRC architecture, the DFRC architecture can be more cost-efficient and has been regarded as one of the most promising directions in B5G era [8].

Meanwhile, the massive multi-input multi-output (MIMO) technology has been proposed as a spectral efficiency (SE) enabler, which facilitates that multiple users share the same time-frequency resource with limited inter-user interference [9]. An emerging massive MIMO architecture, named Cell-Free massive MIMO [10], draws increasing attention, where all antennas which would be collocated on a single traditional BS are geographically distributed over multiple access points (APs) which are connected to a central processing unit (CPU). The Cell-Free massive MIMO system has been shown effective to significantly improve the median wireless coverage performance including both SE and energy efficiency (EE) [11]. Besides, the massive MIMO technology is capable of providing high resolution radar sensing [12]. Therefore, it is attractive to integrate the Cell-Free massive MIMO and the ISAC into a single system, termed the Cell-Free massive MIMO ISAC system.

On the other hand, a trade-off exists in the ISAC system as the two functions for communication and radar sensing

share the available resources, including spectrum bandwidth, power budget and transmit antennas (referred to as spatial degree of freedom) et al. Most existing works concentrated on the communication/radar sensing performance under respective design requirements. The former is termed as the communication-centric design and the latter as the sensing-centric design. Nevertheless, few existing works focused on the study of the entire operation region of the dual functionalities. Besides, in [13], it was verified that by utilizing some wireless coverage enablers, the trade-off can be improved. Moreover, in [14], it was illustrated that the distributed ISAC system can be more cost-effective than the traditional cellular ISAC system in the term of energy consumption. In view of the advantages of the Cell-Free massive MIMO, it is worthwhile to further explore the trade-off in Cell-Free massive MIMO ISAC systems.

B. Related Works

There have been extensive existing works on ISAC systems, see e.g., [15], [16], [17], [18], [19], [20], [21], [22], [23]. In [15], the radar signal-to-interference-plus-noise ratio (SINR) was defined and maximized under the constraints of the power budget and the quality of service (QoS) requirements of users for a CRC system. In [16], a transmit design was investigated with the aim to maximize the communication SINR for a double reconfigurable intelligent surfaces (RISs)-assisted CRC system, and it was illustrated that with the help of RISs, the communication performance can be improved while satisfying the radar sensing requirement. To reduce the hardware costs in ISAC systems, some works adopted the DFRC architecture. In [17] and [18], the sensing-centric hybrid beamforming design was studied for DFRC systems to maximize the sensing performance under the QoS requirements, where the beampattern matching mean square error (MSE) and the Cramér-Rao bound (CRB) were used as the sensing criteria, respectively. In [19], a coordinated cellular network-supported multistatic radar architecture was studied, based on which the sensing beampattern matching MSE was minimized. Apart from sensing-centric designs, some works considered the communication-centric designs in DFRC systems. In [20], a RIS-assisted single-user DFRC system was investigated, where the user's signal-to-noise ratio (SNR) was maximized under the detection probability constraint of radar sensing. In [21], the sum secrecy rate of the network was maximized under the constraint of the radar SNR for a non-orthogonal multiple access (NOMA)-assisted DFRC system. However, the trade-off between communication and radar sensing in ISAC has not yet been reported comprehensively in above mentioned designs. In [22], the communication-sensing (C-S) region was defined and derived for a single-target DFRC system, where the sum rate and the signal-clutter-noise ratio (SCNR) were respectively utilized as the performance metrics for communication and sensing. In [23], the C-S region was obtained for a rate-splitting multiple access-assisted DFRC system where the sum rate and the squared position error bound (SPEB) were respectively employed as the performance metrics for communication and sensing.

The system models in [15], [16], [17], [18], [19], [20], [21], [22], and [23] were based on the traditional cellular architecture. Recently, Cell-Free massive MIMO has been regarded as a promising candidate for the future mobile communication thanks to its superior coverage and high SE. The channel hardening effect in massive MIMO systems relies on the available statistics of the estimated channel [24], thereby making the pilot training of foremost importance. Due to the massive separately distributed APs, the pilot training is challenging in the Cell-Free massive MIMO system [25]. The joint pilot training and information transmission designs have been investigated in many existing works on Cell-Free massive MIMO, see, e.g. [26], [27], [28], [29]. In [26], a channel estimation approach was proposed for a RIS-assisted Cell-Free massive MIMO system with spatially-correlated channels, together with its achievable communication performance. In [27], a downlink EE maximization transmit design was proposed for a Cell-Free massive MIMO system, where the beamforming vectors were designed via maximum ratio transmission (MRT) scheme based on the uplink pilot training. In [28], the MRT scheme was also considered, based on which the SE for a Cell-Free massive MIMO system was maximized and analyzed. In [29], the uplink transmission SE was analyzed for a Cell-Free massive MIMO system by means of the zero-forcing (ZF) scheme and estimated channel.

To enhance the wireless convergence performance for the ISAC system, some papers investigated the integration of Cell-Free massive MIMO and ISAC, see, e.g., [30], [31], [32], [33]. In [30], the sum data rate with the radar estimation performance as constraints was maximized by optimizing the precoding matrix in an orthogonal frequency division multiplexing (OFDM)-based Cell-Free massive MIMO ISAC system. In [31], the radar SNR was maximized under the constraint of the communication SINR requirement in Cell-Free massive MIMO ISAC systems. In [32], the hybrid beamforming design was obtained for Cell-Free ISAC systems with the aim of sum-rate maximization while satisfying the sensing beampattern matching MSE requirement. However, the pilot training phase was not involved in [30], [31], and [32]. In [33], the statistics of the estimated channel were derived via pilot training and then utilized to design the joint uplink communication and sensing scheme for Cell-Free massive MIMO ISAC systems. Nevertheless, [33] did not take the impact of the uncertainty of the target location on the propagation of communication signals into account.

C. Main Contributions

So far, how to jointly mathematically model the uplink training and downlink transmission phases in the Cell-Free massive MIMO ISAC system has never been reported in the open literature. To fill this gap, this paper firstly presents a system model formulation for the Cell-Free massive MIMO ISAC system. It is noticeable that the propagation of wireless signals is more complicated in the Cell-Free massive MIMO ISAC system than that in traditional Cell-Free massive MIMO systems, as the wireless signals will be reflected by location-unknown targets during both uplink and downlink phases. Moreover, the

C-S region defined for the Cell-Free massive MIMO ISAC is for an in-depth trade-off study between communication and radar sensing. The main contributions of this paper are summarized as follows:

1) A Cell-Free massive MIMO ISAC system model is proposed, where during the uplink phase, the channel between each AP and each user is estimated based on the pilot signals transmitted by the user and reflected from multiple targets, and during the downlink phase, the APs serve the users based on the estimated channel and perform target sensing based on the prior information of their locations in the meantime. In addition, the main statistics of the MIMO channel estimation error are theoretically derived in the closed-form fashion.

2) The C-S region is defined for the Cell-Free massive MIMO ISAC system, which can be determined from the following three cases for downlink transmit beamforming design: (i) the sensing-only case by minimizing the sensing beampattern matching MSE; (ii) the communication-only case by maximizing the sum rate; (iii) the ISAC case by maximizing the sum rate subject to all the achievable sensing beampattern matching MSE requirements.

3) The transmit beamforming design problems for the three cases are respectively carried out. The sensing-only case can be directly solved as it is convex. The communication-only case is solved by a block coordinate descent (BCD)-based algorithm after the Lagrangian dual transform and the quadratic fractional transform. The ISAC case is first reformulated similar to the communication-only case, and then solved by a successive convex approximation (SCA) based algorithm in a BCD manner.

4) Numerical results are provided to demonstrate the C-S region, including the C-S performance trade-off characteristics and its impacts with regard to the system parameters, and a comparison with the traditional cellular system. Moreover, the efficacy of the proposed joint C-S transmit beamforming scheme is validated together with its superior performance over the ZF scheme and the MRT scheme.

The rest of the paper is organized as follows. Section II formulates the system model and defines the C-S region. Section III presents a pilot allocation scheme and a target-AP pairing scheme. Section IV solves the correspondng problems to obtain the C-S region. Section V shows the numerical results. Section VI concludes the paper.

Notations: In this paper, x, $\mathbf{x}$, $\mathbf{X}$ and $\mathcal{X}$ are respectively denoted by scalar, vector, matrix and set. $\mathrm{Re}\{\cdot\}$ denotes the real part of a complex number or vector. $|\cdot|$ denotes the absolute value of a complex scalar. $||\cdot||$ denotes the two-norm for a complex vector. $(\cdot)^T$, $(\cdot)^*$ and $(\cdot)^H$ denote the transpose, conjugate and conjugate transpose, respectively. $\mathbb{C}^M$ and $\mathbb{C}^{M\times N}$ denote the set of $M\times 1$ complex-valued vectors and $M\times N$ complex-valued matrices, respectively. $\mathbf{X}\succeq\mathbf{0}$ denotes $\mathbf{X}$ is a positive semidefinite matrix. $\mathbf{a}\sim\mathcal{CN}(\boldsymbol{\mu},\boldsymbol{\Sigma})$ denotes that $\mathbf{a}$ is a complex valued circularly symmetric Gaussian random variable with mean $\boldsymbol{\mu}$ and covariance matrix $\boldsymbol{\Sigma}$. $\mathbb{E}\{\cdot\}$ denotes the expectation for a random variable. $\{\mathbf{x}_{ij}\}$ and $\{\mathbf{x}_{ij}\}_i$ denote all admissible $\{i,j\}$ for $\mathbf{x}_{ij}$ and all admissible i for $\mathbf{x}_{ij}$ with fixed j, respectively.

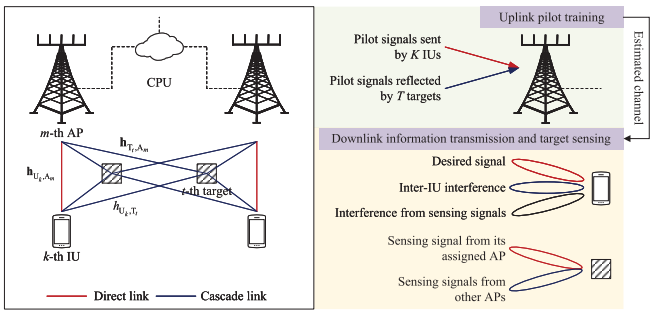

Fig. 1. A cell-free massive MIMO ISAC system.

II. System Model and Communication-Sensing Region Formulation

Consider a Cell-Free Massive MIMO ISAC system as shown in Figure 1, where a CPU coordinates M N_{T}-antenna APs to jointly serve K single-antenna information users (IUs) and detect T point-like device-free targets over the same time and frequency resource. The considered system operates in a time-division duplex mode and each coherence interval is enough to cover τ_{c} symbols, constituted by τ_{p} symbols for uplink pilot training and $(\tau_{\mathrm{c}}-\tau_{\mathrm{p}})$ symbols for downlink information transmission and target sensing. Besides, the signals transmitted by IUs and APs can also be reflected by targets during both uplink and downlink phases. For clarity, let $\mathcal{M}\triangleq\{1,2,\ldots,M\}$, $\mathcal{K}\triangleq\{1,2,\ldots,K\}$ and $\mathcal{T}\triangleq\{1,2,\ldots,T\}$ denote the sets of APs, IUs and targets, respectively.

A. Channel Model

The quasi-static block fading model is adopted, that is, the channels are static and frequency flat in each coherence interval. The distance-dependent path-loss function denoted by $\beta(\cdot)$ can be expressed as [34]

$$\beta(d)=10^{-(128.1+37.6\log_{10}(d))/20}, \tag{1}$$

where d denotes the distance between the transceivers. The channel between the m-th AP and the k-th IU is given by

$$\mathbf{h}_{\mathrm{U}_k,\mathrm{A}_m}=\beta\left(d_{\mathrm{U}_k,\mathrm{A}_m}\right)\mathbf{q}_{\mathrm{U}_k,\mathrm{A}_m}, \tag{2}$$

where $d_{\mathrm{U}_k,\mathrm{A}_m}\triangleq\sqrt{(x_{\mathrm{U}_k}-x_{\mathrm{A}_m})^2+(y_{\mathrm{U}_k}-y_{\mathrm{A}_m})^2}$ denotes the distance between the k-th IU and the m-th AP with $(x_{\mathrm{U}_k},y_{\mathrm{U}_k})$ and $(x_{\mathrm{A}_m},y_{\mathrm{A}_m})$ denoting the coordinates of the k-th IU and the m-th AP, respectively; $\mathbf{q}_{\mathrm{U}_k,\mathrm{A}_m}\in\mathbb{C}^{N_{\mathrm{T}}}$ represents small-scale Rayleigh fading, i.e., $\mathbf{q}_{\mathrm{U}_k,\mathrm{A}_m}\sim\mathcal{CN}(\mathbf{0},\mathbf{I}_{N_{\mathrm{T}}})$.

In practice, the coordinates of the targets may not be exactly known. Based on the pre-detected technology [35] or the location information of targets estimated in the last sensing phase [36], the APs can have prior knowledge of the t-th target's coordinate, denoted by $(\bar{x}_{\mathrm{T}_t},\bar{y}_{\mathrm{T}_t})$. The channel between the m-th AP and the t-th target is modeled as

$$\mathbf{h}_{\mathrm{T}_t,\mathrm{A}_m}=\beta(d_{\mathrm{T}_t,\mathrm{A}_m})\mathbf{q}_{\mathrm{T}_t,\mathrm{A}_m}, \tag{3}$$

where $d_{\mathrm{T}_t,\mathrm{A}_m}$ denotes the distance between the t-th target and the m-th AP, and it is assumed that

$$\beta(d_{\mathrm{T}_t,\mathrm{A}_m}) \sim \mathcal{N}(\beta(\bar{d}_{\mathrm{T}_t,\mathrm{A}_m}), \sigma^2_{\mathrm{T}_t,\mathrm{A}_m})$$

in which $\bar{d}_{\mathrm{T}_t,\mathrm{A}_m} \triangleq \sqrt{(\bar{x}_{\mathrm{T}_t} - x_{\mathrm{A}_m})^2 + (\bar{y}_{\mathrm{T}_t} - y_{\mathrm{A}_m})^2}$; $\mathbf{q}_{\mathrm{T}_t,\mathrm{A}_m} \sim \mathcal{CN}(\bar{\mathbf{q}}_{\mathrm{T}_t,\mathrm{A}_m}, \chi^2_{\mathrm{T}_t,\mathrm{A}_m}\mathbf{I}_{N_\mathrm{T}})$ denotes the steering vector between the t-th target and the m-th AP provided that the sensing channel is line of sight [37], where the steering vector $\bar{\mathbf{q}}_{\mathrm{T}_t,\mathrm{A}_m}$ is given by

$$\bar{\mathbf{q}}_{\mathrm{T}_t,\mathrm{A}_m} = (1, e^{j2\pi\frac{d}{\lambda}\sin(\theta_{tm})}, \ldots, e^{j2\pi\frac{d}{\lambda}(N_\mathrm{T}-1)\sin(\theta_{tm})}) \in \mathbb{C}^{N_\mathrm{T}},$$

in which d and λ denote the spacing between two adjacent antennas and the wavelength of the signal, and θ_{tm} denotes the direction of arrival (DOA) from the m-th AP to the t-th target, where

$$\theta_{tm} = \arccos \frac{y_{\mathrm{A}_m} - \bar{y}_{\mathrm{T}_t}}{\sqrt{(x_{\mathrm{A}_m} - \bar{x}_{\mathrm{T}_t})^2 + (y_{\mathrm{A}_m} - \bar{y}_{\mathrm{T}_t})^2}}. \quad (4)$$

As previously mentioned, the targets may reflect the signals from/to IUs. The channel between the t-th target and the k-th IU is given by

$$h_{\mathrm{U}_k,\mathrm{T}_t} = \beta(d_{\mathrm{U}_k,\mathrm{T}_t}) q_{\mathrm{U}_k,\mathrm{T}_t}, \quad (5)$$

where $d_{\mathrm{U}_k,\mathrm{T}_t}$ denotes the distance between the t-th target and the k-th IU; $q_{\mathrm{U}_k,\mathrm{T}_t} \sim \mathcal{CN}(0,1)$ represents Rayleigh fading between the t-th target and the k-th IU. Similarly, it is assumed $\beta(d_{\mathrm{U}_k,\mathrm{T}_t}) \sim \mathcal{N}(\beta(\bar{d}_{\mathrm{U}_k,\mathrm{T}_t}), \sigma^2_{\mathrm{U}_k,\mathrm{T}_t})$, where $\bar{d}_{\mathrm{U}_k,\mathrm{T}_t} \triangleq \sqrt{(x_{\mathrm{U}_k} - \bar{x}_{\mathrm{T}_t})^2 + (y_{\mathrm{U}_k} - \bar{y}_{\mathrm{T}_t})^2}$.

B. Uplink Pilot Training

In the uplink pilot training phase, the k-th IU transmits a pilot sequence of τ_p symbols to APs to facilitate the channel estimation. To enhance the utilization of the pilot sequence, it is assumed that $\tau_\mathrm{p} < K$, indicating that the pilot sequence must be reused. Denote $\mathcal{P}_k$ by the set of indices of the IUs that share the same pilot sequence with the k-th IU. Note that if the k-th IU shares the same pilot sequence with the k'-th IU, it holds that $\mathcal{P}_k = \mathcal{P}_{k'}$. Let $\sqrt{\tau_\mathrm{p}}\boldsymbol{\phi}_k \in \mathbb{C}^{\tau_\mathrm{p}}$ with $\|\boldsymbol{\phi}_k\|^2 = 1$ denote the pilot sequence allocated to the k-th IU, with the following property:

$$\boldsymbol{\phi}_{k'}^H \boldsymbol{\phi}_k = \begin{cases} 1, & \text{if } k' \in \mathcal{P}_k, \\ 0, & \text{if } k' \notin \mathcal{P}_k. \end{cases}$$

Then, the received signal at the m-th AP can be expressed as

$$\mathbf{Y}_{\mathrm{p},m} = \sum_{k\in\mathcal{K}} \sqrt{p_\mathrm{p}\tau_\mathrm{p}} \left(\mathbf{h}_{\mathrm{U}_k,\mathrm{A}_m} + \sum_{t\in\mathcal{T}} \alpha_t h_{\mathrm{U}_k,\mathrm{T}_t} \mathbf{h}_{\mathrm{T}_t,\mathrm{A}_m} \right) \boldsymbol{\phi}_k^H + \mathbf{N}_{\mathrm{p},m}, \quad (6)$$

where p_p denotes the normalized SNR of each pilot symbol; α_t denotes the reflection coefficient of the t-th target since it can reflect the signals transmitted by IUs; $\mathbf{N}_{\mathrm{p},m} \in \mathbb{C}^{N_\mathrm{T}\times\tau_\mathrm{p}}$ denotes the normalized additive white Gaussian noise (AWGN) at the m-th AP and all the elements of $\mathbf{N}_{\mathrm{p},m}$ are independent identically distributed (i.i.d.) with the distribution $\mathcal{CN}(0,1)$.

To estimate the channel between the m-th AP and the k-th IU, the received signal in (6) can be projected on $\boldsymbol{\phi}_k$ as follows

$$\mathbf{y}_{\mathrm{p},mk} \triangleq \mathbf{Y}_{\mathrm{p},m}\boldsymbol{\phi}_k = \sqrt{p_\mathrm{p}\tau_\mathrm{p}}\mathbf{h}_{mk} + \sum_{k'\in\mathcal{P}_k\setminus\{k\}} \sqrt{p_\mathrm{p}\tau_\mathrm{p}}\mathbf{h}_{mk'} + \mathbf{n}_{\mathrm{p},mk}, \quad (7)$$

where $\mathbf{h}_{mk} \triangleq \mathbf{h}_{\mathrm{U}_k,\mathrm{A}_m} + \sum_{t\in\mathcal{T}} \alpha_t h_{\mathrm{U}_k,\mathrm{T}_t}\mathbf{h}_{\mathrm{T}_t,\mathrm{A}_m}$ denotes the aggregated channel between the m-th AP and k-th IU which includes one direct link and T cascade links; $\mathbf{n}_{\mathrm{p},mk} \triangleq \mathbf{N}_{\mathrm{p},m}\boldsymbol{\phi}_k \sim \mathcal{CN}(\mathbf{0}, \mathbf{I}_{N_\mathrm{T}})$ denotes the projection of $\mathbf{N}_{\mathrm{p},m}$ on $\boldsymbol{\phi}_k$. Instead of estimating $\mathbf{h}_{\mathrm{U}_k,\mathrm{A}_m}, h_{\mathrm{U}_k,\mathrm{T}_t}$ and $\mathbf{h}_{\mathrm{T}_t,\mathrm{A}_m}$ separately, we estimate the aggregated channel $\mathbf{h}_{mk}$, which is more suitable for practical implementation without affecting the downlink transmission. To facilitate channel estimation, the cross-correlation matrix of any two aggregated channels is given in the following proposition.

Proposition 1: Let $\{\mathbf{h}_{mk}\}$ be the aggregated channel defined in (7). Then

$$\mathbb{E}\{\mathbf{h}_{mk}\mathbf{h}_{m'k'}^H\} = \begin{cases} \boldsymbol{\Phi}_{mk}, & \text{if } m' = m,\ k' = k, \\ \boldsymbol{\Phi}_{mm'k}, & \text{if } m' \neq m,\ k' = k, \\ \mathbf{0}, & \text{otherwise}, \end{cases}$$

where $\boldsymbol{\Phi}_{mk}$ and $\boldsymbol{\Phi}_{mm'k}$ are given in (8) and (9), as shown at the bottom of the next page, respectively,

Proof: The proof is given in Appendix A. ∎

By applying the linear minimum MSE method [38], the estimation of the aggregated channel between the k-th IU and m-th AP, denoted by $\widehat{\mathbf{h}}_{mk}$, can be expressed as

$$\widehat{\mathbf{h}}_{mk} = \underbrace{\mathbb{E}\{\mathbf{h}_{mk}\mathbf{y}_{\mathrm{p},mk}^H\}\mathbb{E}^{-1}\{\mathbf{y}_{\mathrm{p},mk}\mathbf{y}_{\mathrm{p},mk}^H\}}_{\triangleq\mathbf{C}_{mk}}\mathbf{y}_{\mathrm{p},mk}. \quad (10)$$

Proposition 2: The mean and auto-correlation matrix of the channel estimations $\{\widehat{\mathbf{h}}_{mk}\}$ defined in (10) are given by

$$\mathbb{E}\{\widehat{\mathbf{h}}_{mk}\} = \mathbf{0} \text{ and } \mathbb{E}\{\widehat{\mathbf{h}}_{mk}\widehat{\mathbf{h}}_{mk}^H\} = \sqrt{p_\mathrm{p}\tau_\mathrm{p}}\mathbf{C}_{mk}\boldsymbol{\Phi}_{mk},$$

respectively, and $\mathbf{C}_{mk}$ defined in (10) can be expressed in a closed form as follows

$$\mathbf{C}_{mk} = \sqrt{p_\mathrm{p}\tau_\mathrm{p}}\boldsymbol{\Phi}_{mk}\left(p_\mathrm{p}\tau_\mathrm{p}\sum_{k'\in\mathcal{P}_k}\boldsymbol{\Phi}_{mk'} + \mathbf{I}_{N_\mathrm{T}}\right)^{-1}.$$

Proof: The proof is given in Appendix B. ∎

Define the channel estimation error as

$$\mathbf{e}_{mk} \triangleq \mathbf{h}_{mk} - \widehat{\mathbf{h}}_{mk}, \quad (11)$$

and its mean and second-order statistics are analyzed in the following proposition.

Proposition 3: The mean and cross-correlation matrix of the channel estimation error $\{\mathbf{e}_{mk}\}$ defined in (11) are given as follows

$$\mathbb{E}\{\mathbf{e}_{mk}\} = \mathbf{0}, \text{ and } \mathbb{E}\{\mathbf{e}_{mk}\mathbf{e}_{m'k}^H\} = \begin{cases} \boldsymbol{\Theta}_{mk}, & \text{if } m' = m, \\ \boldsymbol{\Theta}_{mm'k}, & \text{if } m' \neq m, \end{cases}$$

where $\boldsymbol{\Theta}_{mk} \triangleq \boldsymbol{\Phi}_{mk} - \sqrt{p_\mathrm{p}\tau_\mathrm{p}}\mathbf{C}_{mk}\boldsymbol{\Phi}_{mk}$ and $\boldsymbol{\Theta}_{mm'k}$ is given in (12), as shown at the bottom of the next page.

Proof: The proof is given in Appendix C. ■

Once one realization of $\mathbf{y}_{\mathrm{p},mk}$ is received at the m-th AP, the corresponding channel estimation $\widehat{\mathbf{h}}_{mk}$ can be obtained via (10) and Proposition 2. Next, let us use the obtained $\{\widehat{\mathbf{h}}_{mk}\}$ and the first-order and second-order statistics of $\{\mathbf{e}_{mk}\}$ provided in Proposition 3 to investigate the performance of downlink information transmission and target sensing.

C. Downlink Information Transmission and Target Sensing

In the downlink phase, the APs operate in the dual-function mode, i.e., information transmission and target sensing. Besides, in order to simplify the sensing signal processing and reduce the signal synchronization overhead, we assume that each target is assigned to a single AP to sense[1] and each AP senses at most one target. Generally, the number of APs is larger than that of targets in the Cell-Free system, i.e., $M > T$. Therefore, there may exist some APs only performing the information transmission. Let $\mathcal{M}_{\mathrm{T}}$ ($\mathcal{M}_{\mathrm{I}}$) denotes the set of APs with (without) the target sensing task,[2] namely, $\mathcal{M}_{\mathrm{T}} \cup \mathcal{M}_{\mathrm{I}} = \mathcal{M}$ and $\mathcal{M}_{\mathrm{T}} \cap \mathcal{M}_{\mathrm{I}} = \varnothing$.

For the m-th AP in $\mathcal{M}_{\mathrm{I}}$, the transmit signal is given by

$$\mathbf{x}_m = \sqrt{p_m} \sum_{k\in\mathcal{K}} \mathbf{w}_{mk} s_k, \ \forall m \in \mathcal{M}_{\mathrm{I}}, \tag{13}$$

where p_m denotes the normalized signal power in the downlink phase; $s_k \in \mathbb{C}$ denotes the data symbol intended for the k-th IU with $\mathbb{E}\{|s_k|^2\} = 1$; $\mathbf{w}_{mk} \in \mathbb{C}^{N_{\mathrm{T}}}$ denotes the corresponding beamforming vector. The normalized power budget of the m-th AP is given by $\mathbb{E}\left\{||\mathbf{x}_m||^2\right\} \le p_m$, and thus, it holds that

$$\sum_{k\in\mathcal{K}} \mathbf{w}_{mk}^H \mathbf{w}_{mk} \le 1, \ \forall m \in \mathcal{M}_{\mathrm{I}}. \tag{14}$$

For the m-th AP in $\mathcal{M}_{\mathrm{T}}$, the transmit signal is given by

$$\mathbf{x}_m = \sqrt{p_m} \sum_{k\in\mathcal{K}} \mathbf{w}_{mk} s_k + \sqrt{p_m}\mathbf{z}_m, \ \forall m \in \mathcal{M}_{\mathrm{T}}, \tag{15}$$

[1]The considered system works in a multi-static manner [19]. Although the sensing signal for one target is generated by its assigned AP, the echo signals reflected by the target can be received by all APs and fed back to the CPU for further processing. Besides the dedicated sensing signal, other signals (including communication signals and sensing signals for other targets) may be useful for sensing the target [21] as the Cell-Free massive MIMO system is centralized.

[2]For $m \in \mathcal{M}_{\mathrm{T}}$, the number of streams is $(K+1)$, i.e., K communication signals and 1 sensing signal. For $m \in \mathcal{M}_{\mathrm{I}}$, the number of streams is K, i.e., K communication signals. As for the whole system, the number of streams is $(K+T)$, i.e., K communication signals and T sensing signals.

where $\mathbf{z}_m \in \mathbb{C}^{N_{\mathrm{T}}}$ is the dedicated random sensing signal transmitted by the m-th AP, which is statistically independent of the data symbols $\{s_k\}$ with $\mathbb{E}\{\mathbf{z}_m\mathbf{z}_m^H\} = \mathbf{Z}_m$. Note that the AP generates sensing signal in potential directions of targets. However, only the estimated locations of the targets are available, and the exact distance between each target and its associated AP is unknown. Therefore, in order to achieve the best sensing performance, each AP has to use its utmost power, to enlarge its probing range. Thus, we have

$$\begin{aligned}\mathbb{E}\{||\mathbf{x}_m||^2\} = p_m \\ \Rightarrow \sum_{k\in\mathcal{K}} \mathbf{w}_{mk}^H \mathbf{w}_{mk} + \mathrm{Tr}\{\mathbf{Z}_m\} = 1, \forall m \in \mathcal{M}_{\mathrm{T}}.\end{aligned} \tag{16}$$

The received signal at the k-th IU is the superposition of the signals transmitted by all the APs, which, according to (13) and (15), can be expressed as

$$\begin{aligned} y_{\mathrm{d},k} &= \sum_{m\in\mathcal{M}} \mathbf{h}_{mk}^H \mathbf{x}_m + n_{\mathrm{d},k} \\ &= \sum_{m\in\mathcal{M}} \sqrt{p_m}\widehat{\mathbf{h}}_{mk}^H \mathbf{w}_{mk} s_k + \sum_{m\in\mathcal{M}} \sqrt{p_m}\mathbf{e}_{mk}^H \mathbf{w}_{mk} s_k \\ &\quad + \sum_{k'\neq k} \sum_{m\in\mathcal{M}} \sqrt{p_m}\left(\widehat{\mathbf{h}}_{mk}^H \mathbf{w}_{mk'} s_{k'} + \mathbf{e}_{mk}^H \mathbf{w}_{mk'} s_{k'}\right) \\ &\quad + \sum_{m\in\mathcal{M}_{\mathrm{T}}} \sqrt{p_m}\left(\widehat{\mathbf{h}}_{mk}^H \mathbf{z}_m + \mathbf{e}_{mk}^H \mathbf{z}_m\right) + n_{\mathrm{d},k}, \end{aligned} \tag{17}$$

where $n_{\mathrm{d},k} \in \mathcal{CN}(0,1)$ denotes the normalized AWGN at the k-th IU. Due to the presence of random channel errors $\{\mathbf{e}_{mk}\}$ in the received signal $y_{\mathrm{d},k}$ (cf. (17)), the design of $\{\mathbf{w}_{mk}, \mathbf{Z}_m\}$ is almost prohibitive. Next, let us present how we proceed with this design.

Similar to [39], a computationally tractable lower bound on the IU's ergodic rate can be derived via Jensen's Inequality over $\mathbf{e}_{mk}$. That is,

$$\mathbb{E}\{\log(1+\mathrm{SINR})\} \ge \log(1 + 1/\mathbb{E}\{1/\mathrm{SINR}\}).$$

Denote $r_k\left(\{\mathbf{w}_{mk}, \mathbf{Z}_m\}\right)$ by the lower bound on the achievable k-th IU's ergodic rate, which is given by

$$r_k\left(\{\mathbf{w}_{mk}, \mathbf{Z}_m\}\right) = \log_2\left(1 + \frac{\left|\sum_{m\in\mathcal{M}} \sqrt{p_m}\widehat{\mathbf{h}}_{mk}^H \mathbf{w}_{mk}\right|^2}{A_k\left(\{\mathbf{w}_{mk}, \mathbf{Z}_m\}\right)}\right),$$

where $A_k\left(\{\mathbf{w}_{mk}, \mathbf{Z}_m\}\right)$ is given in (18), as shown at the bottom of page 7, composed of the inter-IU interference, other

$$\mathbf{\Phi}_{mk} = \beta^2\left(d_{\mathrm{U}_k,\mathrm{A}_m}\right)\mathbf{I}_{N_{\mathrm{T}}} + \sum_{t\in\mathcal{T}} \left(\alpha_t^2\left(\beta^2\left(\bar{d}_{\mathrm{U}_k,\mathrm{T}_t}\right) + \sigma_{\mathrm{U}_k,\mathrm{T}_t}^2\right)\left(\beta^2(\bar{d}_{\mathrm{T}_t,\mathrm{A}_m}) + \sigma_{\mathrm{T}_t,\mathrm{A}_m}^2\right) \times \left(\bar{\mathbf{q}}_{\mathrm{T}_t,\mathrm{A}_m}\bar{\mathbf{q}}_{\mathrm{T}_t,\mathrm{A}_m}^H + \chi_{\mathrm{T}_t,\mathrm{A}_m}^2\mathbf{I}_{N_{\mathrm{T}}}\right)\right) \tag{8}$$

$$\mathbf{\Phi}_{mm'k} = \sum_{t\in\mathcal{T}} \alpha_t^2\left(\beta^2\left(\bar{d}_{\mathrm{U}_k,\mathrm{T}_t}\right) + \sigma_{\mathrm{U}_k,\mathrm{T}_t}^2\right)\beta(\bar{d}_{\mathrm{T}_t,\mathrm{A}_m})\beta(\bar{d}_{\mathrm{T}_t,\mathrm{A}_{m'}})\bar{\mathbf{q}}_{\mathrm{T}_t,\mathrm{A}_m}\bar{\mathbf{q}}_{\mathrm{T}_t,\mathrm{A}_{m'}}^H \tag{9}$$

$$\mathbf{\Theta}_{mm'k} \triangleq \mathbf{\Phi}_{mm'k} - \sqrt{p_{\mathrm{p}}\tau_{\mathrm{p}}}\mathbf{\Phi}_{mm'k}\mathbf{C}_{m'k}^H - \sqrt{p_{\mathrm{p}}\tau_{\mathrm{p}}}\mathbf{C}_{mk}\mathbf{\Phi}_{mm'k} + p_{\mathrm{p}}\tau_{\mathrm{p}}\mathbf{C}_{mk}\sum_{k'\in\mathcal{P}_k}\mathbf{\Phi}_{mm'k'}\mathbf{C}_{m'k}^H \tag{12}$$

interference terms induced from the channel estimation errors and/or sensing signals, and AWGN.

Denote the set of targets assigned to the m-th AP by $\mathcal{T}_m$, for which $\mathcal{T}_m = \varnothing$ for all $m \in \mathcal{M}_{\mathrm{I}}$ and $\mathcal{T}_m$ is non-empty for all $m \in \mathcal{M}_{\mathrm{T}}$. Empirically, the best sensing performance of an AP can be obtained when the target is at the direction with maximum gain of its antennas beampattern [40]. Based on such an observation, one AP is assigned to sense at most one target as the number of APs is usually larger than that of the targets. That is, $|\mathcal{T}_m| = 1$, $\forall m \in \mathcal{M}_{\mathrm{T}}$. Provided that the t-th target is the element of $\mathcal{T}_m$, the m-th AP senses the t-th target based on the priori knowledge of the DOA (also known as the DOA estimation), i.e., θ_{tm}, which can be obtained by (4). Particularly, θ_{tm} is utilized to guide the generation of the m-th AP's beampattern. For a direction $\theta \in [-\pi/2, \pi/2]$ of an AP, the steering vector can be expressed as $\mathbf{a}(\theta) = [1, e^{j2\pi \frac{d}{\lambda}\sin(\theta)}, \ldots, e^{j2\pi(N_{\mathrm{T}}-1)\frac{d}{\lambda}\sin(\theta)}]^T$. Then, the amplitude of the m-th AP's beampattern in the direction θ can be expressed as [40]

$$P_m(\theta) = \mathbb{E}\left\{\left|\mathbf{a}^H(\theta)\mathbf{x}_m\right|^2\right\} = p_m \sum_{k\in\mathcal{K}} \left|\mathbf{a}^H(\theta)\mathbf{w}_{mk}\right|^2 + p_m \mathbf{a}^H(\theta)\mathbf{Z}_m\mathbf{a}(\theta). \quad (19)$$

Intuitively, the AP should concentrate its power on the potential directions of its assigned target such that the sensing signal can cover the target. In [41], one kind of ideal beampatterns is mathematically given by

$$\widetilde{P}_m(\theta) = \begin{cases} 1, & |\theta - \theta_{tm}| \le \dfrac{\Delta\theta}{2}, \\ 0, & \text{otherwise}, \end{cases}$$

where $\Delta\theta$ denotes the width (measured by degree) of the ideal beampattern, which is pre-given based on the ISAC scheme according to location uncertainty of targets, number of antennas, etc [19].

A practical beampattern design [42] is adopted for each AP in $\mathcal{M}_{\mathrm{T}}$ as follows. Let $\{\bar{\theta}_n\}_{n=1}^N$ be a considered set of N sampled directions over $[-\pi/2, \pi/2]$. The desirable beampattern can be obtained by minimizing the MSE between the generated beampattern and the ideal beampattern, which is denoted by $\mathcal{E}_m(\eta_m, \{\mathbf{w}_{mk}\}, \mathbf{Z}_m)$ and given by (20), as shown at the bottom of the next page, where $\mathcal{N} \triangleq \{1, 2, \ldots, N\}$ denotes the index set of the sampled directions, and η_m denotes the scaling factor.

D. Communication-Sensing Region

Under the ISAC protocol, the communication function and the target sensing function share the available resource of the Cell-Free system including the frequency bandwidth, transmit power budget and spatial degree of freedom [43]. Since the available resource is limited, there exists a trade-off between communication performance and sensing performance. Such an observation motivates us to investigate the *C-S region* to capture the trade-off between the two functionalities. The C-S region is mathematically defined as

$$\mathcal{R}_{\text{C-S}}(\{\phi_k\}, \{\mathcal{T}_m\}) \triangleq \Big\{(S, R) : \{\mathbf{Z}_m\} \succeq \mathbf{0},\ (14), (16),$$
$$S \ge \frac{1}{M_{\mathrm{T}}} \sum_{m\in\mathcal{M}_{\mathrm{T}}} \mathcal{E}_m(\eta_m, \{\mathbf{w}_{mk}\}, \mathbf{Z}_m),$$
$$R \le \sum_{k\in\mathcal{K}} r_k(\{\mathbf{w}_{mk}, \mathbf{Z}_m\})\Big\}, \quad (21)$$

where $M_{\mathrm{T}} = |\mathcal{M}_{\mathrm{T}}|$ denotes the number of APs required for target sensing. Note that $\mathcal{R}_{\text{C-S}}(\{\phi_k\}, \{\mathcal{T}_m\})$ provides all achievable communication and sensing performance for the considered Cell-Free massive MIMO ISAC system. Especially, each boundary point of $\mathcal{R}_{\text{C-S}}(\{\phi_k\}, \{\mathcal{T}_m\})$ represents the optimal communication/sensing performance with given sensing/communication requirement. For clarity of the ensuing presentation, a synoptic development flow chart for the C-S region is given in Figure 2.

The C-S region is achieved by solving the transmit design problems for the following three cases, i.e., the sensing-only case, the communication-only case and the ISAC case.

1) The Sensing-Only Case: This case without any IUs actually corresponds to the special case of $\{\mathbf{w}_{mk}\} = \{\mathbf{0}\}$. The Cell-Free system aims to obtain the optimal sensing performance $S_{\min}$ by solving the following problem:

$$\mathbf{P_1}: S_{\min} \triangleq \min_{\{\eta_m, \mathbf{Z}_m\}} \sum_{m\in\mathcal{M}_{\mathrm{T}}} \frac{\mathcal{E}_m(\eta_m, \{\mathbf{0}\}, \mathbf{Z}_m)}{M_{\mathrm{T}}} \quad (22a)$$
$$\text{s.t. } \mathrm{Tr}\{\mathbf{Z}_m\} = 1,\ \forall m \in \mathcal{M}_{\mathrm{T}}, \quad (22b)$$
$$\mathbf{Z}_m \succeq \mathbf{0},\ \forall m \in \mathcal{M}_{\mathrm{T}}. \quad (22c)$$

2) The Communication-Only Case: This case without any targets actually corresponds to the special case of $\{\mathbf{Z}_m\} = \{\mathbf{0}\}$. The Cell-Free system aims to obtain the optimal communication performance $R_{\max}$ by solving the following problem:

$$\mathbf{P_2}: R_{\max} \triangleq \max_{\{\mathbf{w}_{mk}\}} \sum_{k\in\mathcal{K}} r_k(\{\mathbf{w}_{mk}, \mathbf{0}\}) \quad (23a)$$
$$\text{s.t. } \sum_{k\in\mathcal{K}} \mathbf{w}_{mk}^H \mathbf{w}_{mk} \le 1,\ \forall m \in \mathcal{M}. \quad (23b)$$

3) The ISAC Case: Apart from the previous two cases, this case with IUs and targets co-existing needs to determinate the coupling boundary of the C-S region within $R \in (0, R_{\max})$ and $S \in (S_{\min}, \infty)$ by solving the following problem:

$$\mathbf{P_3}: \max_{\{\eta_m, \mathbf{w}_{mk}, \mathbf{Z}_m\}} \sum_{k\in\mathcal{K}} r_k(\{\mathbf{w}_{mk}, \mathbf{Z}_m\}) \quad (24a)$$
$$\text{s.t. } \sum_{m\in\mathcal{M}_{\mathrm{T}}} \frac{\mathcal{E}_m(\eta_m, \{\mathbf{w}_{mk}\}, \mathbf{Z}_m)}{M_{\mathrm{T}}} \le \delta, \quad (24b)$$
$$\mathbf{Z}_m \succeq \mathbf{0},\ \forall m \in \mathcal{M}_{\mathrm{T}}, \quad (24c)$$
$$(14), (16),$$

where $\delta \in [S_{\min}, \infty)$ is pre-given which denotes the sensing requirement in the term of the average sensing beampattern matching MSE over all targets.[3]

[3]The average sensing beampattern matching MSE represents the global sensing performance. The C-S region can be re-defined based on other communication/sensing metrics. Nevertheless, the processes to derive the C-S region are similar.

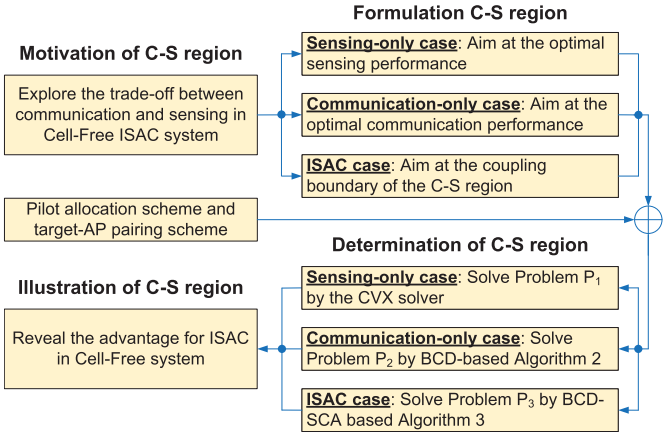

Fig. 2. Synoptic development flow chart for the C-S region.

Remark 1: Alternatively, the C-S region can also be obtained by solving the following problem instead of Problem $\mathbf{P_3}$

$$\mathbf{P_4}: \min_{\{\eta_m, \mathbf{w}_{mk}, \mathbf{Z}_m\}} \sum_{m\in\mathcal{M}_\mathrm{T}} \frac{\mathcal{E}_m\left(\eta_m, \{\mathbf{w}_{mk}\}, \mathbf{Z}_m\right)}{M_\mathrm{T}} \tag{25a}$$

$$\text{s.t.} \sum_{k\in\mathcal{K}} r_k\left(\{\mathbf{w}_{mk}, \mathbf{Z}_m\}\right) \geq \zeta, \tag{25b}$$

$$\mathbf{Z}_m \succeq \mathbf{0}, \ \forall m \in \mathcal{M}_\mathrm{T}, \tag{25c}$$

$$(14), (16),$$

where $\zeta \in (0, R_{\max}]$ *is pre-given which denotes the communication requirement in the term of the sum rate of all IUs.*

Remark 2: Let $\mathbf{bd}\,\mathcal{R}_{C\text{-}S}$ *denote the set of all the boundary points of the C-S region. Then* $(S_{\min}, R_\mathrm{T})$ *and* $(S_\mathrm{I}, R_{\max})$ *are the two critical points of* $\mathbf{bd}\,\mathcal{R}_{C\text{-}S}$*, where* R_T *is the optimal value of Problem* $\mathbf{P_3}$ *under* $\delta = S_{\min}$ *and* S_I *is the optimal value of Problem* $\mathbf{P_4}$ *under* $\zeta = R_{\max}$*. All the points of* $\mathbf{bd}\,\mathcal{R}_{C\text{-}S}$ *between* $(S_{\min}, R_\mathrm{T})$ *and* $(S_\mathrm{I}, R_{\max})$ *can be obtained by solving Problem* $\mathbf{P_3}$ *(Problem* $\mathbf{P_4}$*) subject to an assigned parameter* $\delta \geq S_{\min}$ *(*$\zeta \leq R_{\max}$*), where the C-S performance trade-off occurs due to finite resources. The union of the set* $\{(S, R_{\max}) \mid S > S_I\}$ *and the set* $\{(S_{\min}, R) \mid R < R_T\}$ *contains all the other points of* $\mathbf{bd}\,\mathcal{R}_{C-S}$*.*

As mentioned in Remark 2, to determine the set $\mathcal{R}_{\text{C-S}}$, we need to practically solve Problem $\mathbf{P_1}$, Problem $\mathbf{P_2}$ and Problem $\mathbf{P_3}$ (Problem $\mathbf{P_4}$) after finishing the pilot allocation and target-AP pairing. The schemes for pilot allocation and target-AP pairing are presented in the next section, and all the algorithms needed for determining $\mathcal{R}_{\text{C-S}}$ will be presented in Section IV.

III. Pilot Allocation Scheme and Target-AP Pairing Scheme

Because the *uplink pilot training* depends on the pilot allocation scheme, i.e., $\{\mathcal{P}_k\}$, while the *downlink information transmission and target sensing* depends on the target-AP pairing scheme, i.e., $\{\mathcal{T}_m\}$, a pilot allocation scheme and a target-AP pairing scheme are respectively presented in the following two subsections.

A. Pilot Allocation Scheme

As mentioned above, the number of IUs is greater than the length of the pilot sequence, i.e., $K > \tau_\mathrm{p}$, which makes the pilot contamination is unavoidable. In order to mitigate the pilot contamination, the IUs far away from each other will reuse the same pilot sequence. To this end, a pilot allocation scheme based on the hierarchical agglomerative clustering (HAC) method [44] is designed. First of all, each IU forms one cluster denoted by $\{\mathcal{C}_i\}$, thus forming K one-member clusters. Denote the inter-cluster distance between $\mathcal{C}_i$ and $\mathcal{C}_j$ $(j \neq i)$ by

$$d_{ij} = \min_{k\in\mathcal{C}_i, k'\in\mathcal{C}_j} \left\{\sqrt{(x_{\mathrm{U}_k} - x_{\mathrm{U}_{k'}})^2 + (y_{\mathrm{U}_k} - y_{\mathrm{U}_{k'}})^2}\right\}.$$

Then, two clusters with the maximum inter-cluster distance are merged into one cluster until τ_p clusters survive. Note that if

$$\begin{aligned} A_k\left(\{\mathbf{w}_{mk}, \mathbf{Z}_m\}\right) \triangleq\ & \mathbb{E}\left\{\left|\sum_{m\in\mathcal{M}} \sqrt{p_m}\mathbf{e}_{mk}^H \mathbf{w}_{mk}\right|^2\right\} + \sum_{k'\neq k}\left|\sum_{m\in\mathcal{M}} \sqrt{p_m}\widehat{\mathbf{h}}_{mk}^H \mathbf{w}_{mk'}\right|^2 + \sum_{k'\neq k}\mathbb{E}\left\{\left|\sum_{m\in\mathcal{M}} \sqrt{p_m}\mathbf{e}_{mk}^H \mathbf{w}_{mk'}\right|^2\right\} \\ & + \sum_{m\in\mathcal{M}_\mathrm{T}} p_m \widehat{\mathbf{h}}_{mk}^H \mathbf{Z}_m \widehat{\mathbf{h}}_{mk} + \sum_{m\in\mathcal{M}_\mathrm{T}} p_m \mathbb{E}\left\{\mathbf{e}_{mk}^H \mathbf{Z}_m \mathbf{e}_{mk}\right\} + 1 \\ =\ & \sum_{m\in\mathcal{M}} p_m \mathbf{w}_{mk}^H \mathbf{\Theta}_{mk} \mathbf{w}_{mk} + \sum_{m\in\mathcal{M}}\sum_{m'\neq m} \sqrt{p_m p_{m'}}\mathbf{w}_{mk}^H \mathbf{\Theta}_{mm'k} \mathbf{w}_{m'k} + \sum_{k'\neq k}\left|\sum_{m\in\mathcal{M}} \sqrt{p_m}\widehat{\mathbf{h}}_{mk}^H \mathbf{w}_{mk'}\right|^2 \\ & + \sum_{k'\neq k}\sum_{m\in\mathcal{M}} p_m \mathbf{w}_{mk'}^H \mathbf{\Theta}_{mk} \mathbf{w}_{mk'} + \sum_{k'\neq k}\sum_{m\in\mathcal{M}}\sum_{m'\neq m} \sqrt{p_m p_{m'}}\mathbf{w}_{mk'}^H \mathbf{\Theta}_{mm'k} \mathbf{w}_{m'k'} \\ & + \sum_{m\in\mathcal{M}_\mathrm{T}} p_m \widehat{\mathbf{h}}_{mk}^H \mathbf{Z}_m \widehat{\mathbf{h}}_{mk} + \sum_{m\in\mathcal{M}_\mathrm{T}} p_m \mathrm{Tr}\left\{\mathbf{\Theta}_{mk}\mathbf{Z}_m\right\} + 1 \end{aligned} \tag{18}$$

$$\mathcal{E}_m\left(\eta_m, \{\mathbf{w}_{mk}\}, \mathbf{Z}_m\right) = \frac{1}{N}\sum_{n\in\mathcal{N}}\left|\eta_m \widetilde{P}_m(\bar{\theta}_n) - p_m \mathbf{a}^H(\bar{\theta}_n)\left(\sum_{k\in\mathcal{K}} \mathbf{w}_{mk}\mathbf{w}_{mk}^H + \mathbf{Z}_m\right)\mathbf{a}(\bar{\theta}_n)\right|^2 \tag{20}$$

$k \in \mathcal{C}_i$, it holds that $\mathcal{P}_k = \mathcal{C}_i$. The proposed clustering scheme is summarized in Algorithm 1.

Algorithm 1 The Proposed HAC Algorithm for Pilot Allocation Scheme

Initialization:
Treat each IU as a cluster head and set $num = K$;
Calculate the inter-cluster distance set $\{d_{ij}\}$;
while $num > \tau_{\mathrm{p}}$ **do**
  Merge the two clusters with maximum d_{ij} into one cluster;
  Update $num := num - 1$;
  Update the inter-cluster distnace set $\{d_{ij}\}$;
end
Assign τ_{p} a distinct orthogonal pilot sequence to each of τ_{p} IU clusters.

B. Target-AP Pairing Scheme

As mentioned above, the probing range of each AP is bounded by the power budget. Thus, to obtain a good sensing performance, the AP responsible for sensing the assigned target should be close to the target. However, the exact coordinate of each target is unknown. Therefore, the prior knowledge of the target-AP distances, i.e., $\{\bar{d}_{\mathrm{T}_t,\mathrm{A}_m}\}$ can be employed for target-AP pairing. One intuitive way of the target-AP pairing is to minimize the sum distance between targets and their serving APs. All the APs and targets in the considered system can be treated as a weighted complete bipartite graph $G = (\mathcal{M}, \mathcal{T})$, where $\{-\bar{d}_{\mathrm{T}_t,\mathrm{A}_m}\}$ is the corresponding edge weight between T_t and A_m. Then, the sum distance minimization problem is equivalent to optimal matching problem on G, which can be solved by the Kuhn–Munkres Algorithm [45].

IV. Proposed C-S Region Determination

With the pilot allocation scheme and the target-AP pairing scheme, Problems $\mathbf{P_1}$, $\mathbf{P_2}$ and $\mathbf{P_3}$ need to be respectively solved to obtain the C-S region.

A. Sensing-Only Case

It is observed that $\mathbf{Z}_m$ and $\mathbf{Z}_{m'}$ $(m' \neq m)$ are uncoupled in the convex constraints of Problem $\mathbf{P_1}$ and the objective function of Problem $\mathbf{P_1}$ is also convex. Thus, it can be decomposed into M_{T} convex sub-problems, which can be solved by CVX solvers, e.g., `SDPT3`, in a parallel fashion.

B. Communication-Only Case

From Problem $\mathbf{P_2}$, it can be observed that $\{\mathbf{w}_{mk}\}_k$ and $\{\mathbf{w}_{m'k}\}_k$ $(m' \neq m)$ are uncoupled in the constraints. Therefore, solving Problem $\mathbf{P_2}$ is equivalent to solving M sub-problems, of which the m-th sub-problem is given by

$$\mathbf{P_{2.1}}: \max_{\{\mathbf{w}_{mk}\}_k} \sum_{k\in\mathcal{K}} r_k\left(\{\mathbf{w}_{mk}, \mathbf{0}\}\right) \tag{26a}$$

$$\text{s.t.} \sum_{k\in\mathcal{K}} \mathbf{w}_{mk}^H \mathbf{w}_{mk} \leq 1. \tag{26b}$$

Problem $\mathbf{P_{2.1}}$ can be optimally solved based on the idea of Lagrangian dual transform [46] and quadratic fractional transform [47]. Through the Lagrangian dual transform, Problem $\mathbf{P_{2.1}}$ can be decomposed as an inner optimization problem and an outer optimization problem. With the closed-form optimal solution to the inner optimization problem and the KKT condition, the outer optimization problem can be reformulated. Through the quadratic fractional transform, the variables of the reformulated outer problem are decoupled and can be optimized in a BCD manner. The details are presented as follows.

By introducing auxiliary variables $\boldsymbol{\gamma} = [\gamma_1, \gamma_2, \ldots, \gamma_K]^T$, Problem $\mathbf{P_{2.1}}$ can be re-written as

$$\mathbf{P_{2.2}}: \max_{\boldsymbol{\gamma}, \{\mathbf{w}_{mk}\}_k} \sum_{k\in\mathcal{K}} \log_2\left(1+\gamma_k\right) \tag{27a}$$

$$\text{s.t.} \sum_{k\in\mathcal{K}} \mathbf{w}_{mk}^H \mathbf{w}_{mk} \leq 1, \tag{27b}$$

$$\gamma_k \leq \frac{\left|\sum_{m\in\mathcal{M}} \sqrt{p_m}\widehat{\mathbf{h}}_{mk}^H \mathbf{w}_{mk}\right|^2}{A_k\left(\{\mathbf{w}_{mk}, \mathbf{0}\}\right)}, \ \forall k \in \mathcal{K}. \tag{27c}$$

Similar to [48], with fixed $\{\mathbf{w}_{mk}\}_k$, the inner optimization problem is expressed as

$$\mathbf{P_{2.3}}: \max_{\boldsymbol{\gamma}} \sum_{k\in\mathcal{K}} \log_2\left(1+\gamma_k\right) \tag{28a}$$

$$\text{s.t. } \gamma_k \leq \frac{\left|\sum_{m\in\mathcal{M}} \sqrt{p_m}\widehat{\mathbf{h}}_{mk}^H \mathbf{w}_{mk}\right|^2}{A_k\left(\{\mathbf{w}_{mk}, \mathbf{0}\}\right)}, \ \forall k \in \mathcal{K}, \tag{28b}$$

and the closed-form solution to Problem $\mathbf{P_{2.3}}$, denoted by $\boldsymbol{\gamma}^\star = [\gamma_1^\star, \gamma_2^\star, \ldots, \gamma_K^\star]^T$, is given by

$$\gamma_k^\star = \frac{\left|\sum_{m\in\mathcal{M}} \sqrt{p_m}\widehat{\mathbf{h}}_{mk}^H \mathbf{w}_{mk}\right|^2}{A_k\left(\{\mathbf{w}_{mk}, \mathbf{0}\}\right)}. \tag{29}$$

Since Problem $\mathbf{P_{2.3}}$ is convex, the Slater condition holds, and hence strong duality also holds. Let $\boldsymbol{\lambda} = [\lambda_1, \lambda_2, \ldots, \lambda_K]^T$ be the Lagrangian multiplier associated with constraint (28b), the Lagrangian function of Problem $\mathbf{P_{2.3}}$ is given by

$$\mathcal{L}_1(\boldsymbol{\gamma}, \boldsymbol{\lambda}) = \sum_{k\in\mathcal{K}} \log_2(1+\gamma_k) + \sum_{k\in\mathcal{K}} \lambda_k \left(\frac{\left|\sum_{m\in\mathcal{M}} \sqrt{p_m}\widehat{\mathbf{h}}_{mk}^H \mathbf{w}_{mk}\right|^2}{A_k\left(\{\mathbf{w}_{mk}, \mathbf{0}\}\right)} - \gamma_k \right). \tag{30}$$

Denote $\boldsymbol{\lambda}^\star = [\lambda_1^\star, \lambda_2^\star, \ldots, \lambda_K^\star]^T$ by the optimal solution to the dual problem of Problem $\mathbf{P_{2.3}}$. According to the KKT condition, it holds that

$$\left.\frac{\partial \mathcal{L}_1(\boldsymbol{\gamma}, \boldsymbol{\lambda})}{\partial \gamma_k}\right|_{\boldsymbol{\gamma}=\boldsymbol{\gamma}^\star, \boldsymbol{\lambda}=\boldsymbol{\lambda}^\star} = 0 \Rightarrow \lambda_k^\star = \frac{1}{(1+\gamma_k^\star)\ln 2} = \frac{A_k\left(\{\mathbf{w}_{mk}, \mathbf{0}\}\right)}{\left(A_k\left(\{\mathbf{w}_{mk}, \mathbf{0}\}\right) + \left|\sum_{m\in\mathcal{M}} \sqrt{p_m}\widehat{\mathbf{h}}_{mk}^H \mathbf{w}_{mk}\right|^2\right)\ln 2}. \tag{31}$$

By substituting (31) into (30), Problem $\mathbf{P_{2.2}}$ can be re-expressed as

$$\mathbf{P_{2.4}}: \max_{\boldsymbol{\gamma},\{\mathbf{w}_{mk}\}_k} f_1\left(\boldsymbol{\gamma},\{\mathbf{w}_{mk}\}_k\right) \tag{32a}$$

$$\text{s.t.} \sum_{k\in\mathcal{K}} \mathbf{w}_{mk}^H \mathbf{w}_{mk} \le 1, \tag{32b}$$

where $f_1(\boldsymbol{\gamma},\{\mathbf{w}_{mk}\}_k)$ is given by (33), as shown at the bottom of the next page. Problem $\mathbf{P_{2.4}}$ is non-convex due to the non-concave third term in $f_1(\boldsymbol{\gamma},\{\mathbf{w}_{mk}\}_k)$, which can be further handled via the following lemma based on the quadratic fractional transform.

Lemma 1: Given a feasible set $\mathcal{X}\subseteq\mathbb{C}^n$, a function $F(\mathbf{x}):\mathbb{C}^n\to\mathbb{C}$ and a function $G(\mathbf{x}):\mathbb{C}^n\to\mathbb{R}^+$. Then, the following two problems are equivalent.

$$\mathbf{P_5}: \max_{\mathbf{x}} \ \mu_1(\mathbf{x}) \triangleq \frac{|F(\mathbf{x})|^2}{G(\mathbf{x})}$$
$$\text{s.t. } \mathbf{x}\in\mathcal{X}.$$
$$\mathbf{P_6}: \max_{\mathbf{x},y} \ \mu_2(\mathbf{x},y) \triangleq 2\mathrm{Re}\{y^* F(\mathbf{x})\} - |y|^2 G(\mathbf{x})$$
$$\text{s.t. } \mathbf{x}\in\mathcal{X}, y\in\mathbb{C}.$$

Proof: Observe that Problem $\mathbf{P_6}$ is concave with respect to (w.r.t.) the unconstrained variable y. Therefore, with given $\mathbf{x}$, the optimal $y^\star$ satisfies that $\partial\mu_2(\mathbf{x},y)/\partial y = 0$, which indicates that $y^\star = F(\mathbf{x})/G(\mathbf{x})$. By substituting $y^\star$ into $\mu_2(\mathbf{x},y)$, it holds that $\mu_1(\mathbf{x}) = \mu_2(\mathbf{x},y^\star)$. Then, Problems $\mathbf{P_5}$ and $\mathbf{P_6}$ are equivalent. ∎

With auxiliary variables $\mathbf{g} \triangleq [g_1, g_2, \ldots, g_K]^T$ and by Lemma 1, Problem $\mathbf{P_{2.4}}$ can be rewritten as the following problem

$$\mathbf{P_{2.5}}: \max_{\boldsymbol{\gamma},\{\mathbf{w}_{mk}\}_k,\mathbf{g}} f_2\left(\boldsymbol{\gamma},\{\mathbf{w}_{mk}\}_k,\mathbf{g}\right) \tag{34a}$$

$$\text{s.t.} \sum_{k\in\mathcal{K}} \mathbf{w}_{mk}^H \mathbf{w}_{mk} \le 1, \tag{34b}$$

where $f_2\left(\boldsymbol{\gamma},\{\mathbf{w}_{mk}\}_k,\mathbf{g}\right)$ is given by (35), as shown at the bottom of the next page. As $\mathbf{g}$ is unconstrained and $f_2\left(\boldsymbol{\gamma},\{\mathbf{w}_{mk}\}_k,\mathbf{g}\right)$ is concave w.r.t. $\mathbf{g}$, the optimal $\mathbf{g}^\star = [g_1^\star, g_2^\star, \ldots, g_K^\star]^T$ satisfies $\partial f_2\left(\boldsymbol{\gamma},\{\mathbf{w}_{mk}\}_k,\mathbf{g}\right)/\partial g_k = 0$ with given $\boldsymbol{\gamma}$ and $\{\mathbf{w}_{mk}\}_k$, thereby yielding

$$g_k^\star = \frac{\sqrt{(1+\gamma_k)}\sum_{m\in\mathcal{M}}\sqrt{p_m}\widehat{\mathbf{h}}_{mk}^H\mathbf{w}_{mk}}{A_k\left(\{\mathbf{w}_{mk},\mathbf{0}\}\right) + \left|\sum_{m\in\mathcal{M}}\sqrt{p_m}\widehat{\mathbf{h}}_{mk}^H\mathbf{w}_{mk}\right|^2}. \tag{36}$$

Notice that the first term, the third term and the fourth term in $A_k\left(\{\mathbf{w}_{mk},\mathbf{0}\}\right)$ (cf. (18)) are quadratic w.r.t. $\{\mathbf{w}_{mk}\}_k$. Besides, with given $\{\mathbf{w}_{m'k}\}_{m'\neq m}$, the second term and the fifth term in $A_k\left(\{\mathbf{w}_{mk},\mathbf{0}\}\right)$ are linear w.r.t. $\{\mathbf{w}_{mk}\}_k$. That is, $A_k\left(\{\mathbf{w}_{mk},\mathbf{0}\}\right)$ is convex w.r.t. $\{\mathbf{w}_{mk}\}_k$ with given $\{\mathbf{w}_{m'k}\}_{m'\neq m}$, implying that $f_2\left(\boldsymbol{\gamma},\{\mathbf{w}_{mk}\}_k,\mathbf{g}\right)$ is concave w.r.t. $\{\mathbf{w}_{mk}\}_k$. As a result, $\boldsymbol{\gamma},\{\mathbf{w}_{mk}\}_k$ and $\mathbf{g}$ can be optimized in a BCD manner, since they are decoupled in the constraint of Problem $\mathbf{P_{2.5}}$. Moreover, when other variables are fixed, the closed-form expressions of the optimal $\boldsymbol{\gamma}^\star$ and $\mathbf{g}^\star$ have been obtained in (29) and (36), respectively, while $\{\mathbf{w}_{mk}^\star\}_k$ is optimized by solving

$$\mathbf{P_{2.6}}: \max_{\{\mathbf{w}_{mk}\}_k} f_2\left(\boldsymbol{\gamma},\{\mathbf{w}_{mk}\}_k,\mathbf{g}\right) \tag{37a}$$

$$\text{s.t.} \sum_{k\in\mathcal{K}} \mathbf{w}_{mk}^H \mathbf{w}_{mk} \le 1. \tag{37b}$$

Furthermore, Problem $\mathbf{P_2}$ can also be solved in a parallel fashion instead of solving the M sub-problems sequentially. Finally, by integrating all the preceding approaches, we end up with Algorithm 2 for handling Problem $\mathbf{P_2}$.

Algorithm 2 The Proposed BCD-Based Algorithm for Solving Problem $\mathbf{P_2}$

Initialization:
Find a feasible $\{\mathbf{w}_{mk}\}$ to Problem $\mathbf{P_2}$;
while *the stop criterion is not satified* **do**
  for $m\in\mathcal{M}$ **parallel do**
    Calculate $\boldsymbol{\gamma}$ and $\mathbf{g}$ with $\{\mathbf{w}_{mk}\}$ by (29) and (36), respectively;
    while *the stop criterion is not satified* **do**
      Obtain the optimal solution $\{\mathbf{w}_{mk}^\star\}_k$ by solving Problem $\mathbf{P_{2.6}}$ with $\boldsymbol{\gamma}$, $\mathbf{g}$ and $\{\mathbf{w}_{m'k}\}_{m'\neq m}$;
      Update $\boldsymbol{\gamma}$ with $\{\mathbf{w}_{mk}^\star\}_k$ and $\{\mathbf{w}_{m'k}\}_{m'\neq m}$ by (29);
      Update $\mathbf{g}$ with $\{\mathbf{w}_{mk}^\star\}_k$, $\{\mathbf{w}_{m'k}\}_{m'\neq m}$ and $\boldsymbol{\gamma}$ by (36);
    end
  end
  Update $\{\mathbf{w}_{mk}\} := \{\mathbf{w}_{mk}^\star\}$;
end

By solving Problem $\mathbf{P_{2.6}}$ via a standard interior-point method, the computational complexity of Algorithm 2 is $\mathcal{O}(I_1K^3N_{\mathrm{T}}^3)$, where I_1 denotes the number of required iterations to converge for Algorithm 2.

C. ISAC Case

Similar to the reformations in *the communication-only case*, based on the Lagrangian dual transform and the quadratic fractional transform, the objective function (24a) of Problem $\mathbf{P_3}$ can be rewritten as $f_3\left(\{\mathbf{w}_{mk}\},\{\mathbf{Z}_m\},\boldsymbol{\iota},\boldsymbol{\kappa}\right)$ with auxiliary variables $\boldsymbol{\iota} \triangleq [\iota_1,\iota_2,\ldots,\iota_K]^T$ and $\boldsymbol{\kappa} \triangleq [\kappa_1,\kappa_2,\ldots,\kappa_K]^T$, which is given in (38), as shown at the bottom of the next page. Since $\{\eta_m,\mathbf{w}_{mk},\mathbf{Z}_m\}$, $\boldsymbol{\iota}$ and $\boldsymbol{\kappa}$ are uncoupled in the feasible set, they can also be optimized in a BCD manner. Besides, the closed-form expressions of the optimal $\boldsymbol{\iota}^\star \triangleq [\iota_1^\star,\iota_2^\star,\ldots,\iota_K^\star]^T$ with fixed $\{\mathbf{w}_{mk},\mathbf{Z}_m\}$ and those of the optimal $\boldsymbol{\kappa}^\star \triangleq [\kappa_1^\star,\kappa_2^\star,\ldots,\kappa_K^\star]^T$ with fixed $\{\mathbf{w}_{mk},\mathbf{Z}_m\}$ and $\boldsymbol{\iota}$ are respectively given by

$$\iota_k^\star = \frac{\left|\sum_{m\in\mathcal{M}}\sqrt{p_m}\widehat{\mathbf{h}}_{mk}^H\mathbf{w}_{mk}\right|^2}{A_k\left(\{\mathbf{w}_{mk},\mathbf{Z}_m\}\right)} \tag{39}$$

and

$$\kappa_k^\star = \frac{\sqrt{(1+\iota_k)}\sum_{m\in\mathcal{M}}\sqrt{p_m}\widehat{\mathbf{h}}_{mk}^H\mathbf{w}_{mk}}{A_k\left(\{\mathbf{w}_{mk},\mathbf{Z}_m\}\right) + \left|\sum_{m\in\mathcal{M}}\sqrt{p_m}\widehat{\mathbf{h}}_{mk}^H\mathbf{w}_{mk}\right|^2}. \tag{40}$$

With given $\boldsymbol{\iota}$ and $\boldsymbol{\kappa}$, $\{\eta_m^\star, \mathbf{w}_{mk}^\star, \mathbf{Z}_m^\star\}$ can be obtained through solving the following problem.

$$\mathbf{P_{3.1}}: \max_{\{\eta_m, \mathbf{w}_{mk}, \mathbf{Z}_m\}} f_3\left(\{\mathbf{w}_{mk}\}, \{\mathbf{Z}_m\}, \boldsymbol{\iota}, \boldsymbol{\kappa}\right) \quad \text{s.t.} \quad (14), (16), (24b), (24c). \tag{41a}$$

It is observed that $f_3(\{\mathbf{w}_{mk}\}, \{\mathbf{Z}_m\}, \boldsymbol{\iota}, \boldsymbol{\kappa})$ is non-concave w.r.t. $\{\mathbf{w}_{mk}\}$ since $A_k(\{\mathbf{w}_{mk}, \mathbf{Z}_m\})$ (cf. (18)) is non-convex w.r.t. $\{\mathbf{w}_{mk}\}$.

To tackle the non-concave objective function of Problem $\mathbf{P_{3.1}}$, i.e., $f_3(\{\mathbf{w}_{mk}\}, \{\mathbf{Z}_m\}, \boldsymbol{\iota}, \boldsymbol{\kappa})$, we define convex functions $B_k(\{\mathbf{w}_{mk}, \mathbf{Z}_m\})$ and $C_k(\{\mathbf{w}_{mk}\})$ as (42) and (43), shown at the bottom of the next page, respectively. Then, $A_k(\{\mathbf{w}_{mk}, \mathbf{Z}_m\})$ can be rewritten as

$$A_k\left(\{\mathbf{w}_{mk}, \mathbf{Z}_m\}\right) = B_k\left(\{\mathbf{w}_{mk}, \mathbf{Z}_m\}\right) - C_k\left(\{\mathbf{w}_{mk}\}\right). \tag{44}$$

By introducing auxiliary variables $\mathbf{u} = [u_1, u_2, \ldots, u_K]^T$ in which $u_k = C_k(\{\mathbf{w}_{mk}\})$, and then, substituting $A_k\{\mathbf{w}_{mk}, \mathbf{Z}_m\})$ in $f_3(\{\mathbf{w}_{mk}\}, \{\mathbf{Z}_m\}, \boldsymbol{\iota}, \boldsymbol{\kappa})$ by $(B_k(\{\mathbf{w}_{mk}, \mathbf{Z}_m\}) - u_k)$, Problem $\mathbf{P_{3.1}}$ can be reformulated as

$$\mathbf{P_{3.2}}: \max_{\{\eta_m, \mathbf{w}_{mk}, \mathbf{Z}_m\}, \mathbf{u}} f_4\left(\{\mathbf{w}_{mk}\}, \{\mathbf{Z}_m\}, \boldsymbol{\iota}, \boldsymbol{\kappa}, \mathbf{u}\right) \tag{45a}$$

$$\text{s.t. } u_k \le C_k\left(\{\mathbf{w}_{mk}\}\right), \forall k \in \mathcal{K}, \quad (14), (16), (24b), (24c), \tag{45b}$$

where $f_4\left(\{\mathbf{w}_{mk}\}, \{\mathbf{Z}_m\}, \boldsymbol{\iota}, \boldsymbol{\kappa}, \mathbf{u}\right)$ is a concave function w.r.t. $\{\mathbf{w}_{mk}\}$ given in (46), as shown at the bottom of the next page. However, the constraints (16) and (24b) are still non-convex.

To tackle the non-convex constraint (24b), define $D_{mn}(\eta_m, \{\mathbf{w}_{mk}\}, \mathbf{Z}_m)$ as (47), shown at the bottom of the next page and introduce auxiliary variables $\boldsymbol{\xi} = [\xi_{11}, \xi_{12}, \ldots, \xi_{M_{\mathrm{T}}N}]^T$ in which $\xi_{mn} = |D_{mn}(\eta_m, \{\mathbf{w}_{mk}\}, \mathbf{Z}_m)|$. Then, (24b) can be re-expressed as

$$\xi_{mn} \ge D_{mn}\left(\eta_m, \{\mathbf{w}_{mk}\}, \mathbf{Z}_m\right), \tag{48a}$$

$$-\xi_{mn} \le D_{mn}\left(\eta_m, \{\mathbf{w}_{mk}\}, \mathbf{Z}_m\right), \tag{48b}$$

$$\text{and} \sum_{m \in \mathcal{M}_{\mathrm{T}}} \sum_{n \in \mathcal{N}} \frac{\xi_{mn}^2}{M_{\mathrm{T}} N} \le \delta. \tag{48c}$$

As for (16), by introducing an auxiliary variable $v < 1$ satisfying

$$\sum_{k \in \mathcal{K}} \mathbf{w}_{mk}^H \mathbf{w}_{mk} + \mathrm{Tr}\{\mathbf{Z}_m\} \ge v, \forall m \in \mathcal{M}_{\mathrm{T}}, \tag{49}$$

and embedding a penalty term $(1 - v)$ into the objective function, (16) can be relaxed as follows:

$$\sum_{k \in \mathcal{K}} \mathbf{w}_{mk}^H \mathbf{w}_{mk} + \mathrm{Tr}\{\mathbf{Z}_m\} \le 1, \forall m \in \mathcal{M}_{\mathrm{T}}, \tag{50}$$

As a result, Problem $\mathbf{P_{3.2}}$ is equivalent to the following problem

$$\mathbf{P_{3.3}}: \max_{\{\eta_m, \mathbf{w}_{mk}, \mathbf{Z}_m\}, \mathbf{u}, \boldsymbol{\xi}, v} f_4\left(\{\mathbf{w}_{mk}\}, \{\mathbf{Z}_m\}, \boldsymbol{\iota}, \boldsymbol{\kappa}, \mathbf{u}\right) - q(1 - v)$$

$$\text{s.t.} \quad (14), (24c), (45b), (48a), (48b), (48c), (49), (50), \tag{51a}$$

where q is a positive hyper-parameter in order to enforce $\sum_{k \in \mathcal{K}} \mathbf{w}_{mk}^H \mathbf{w}_{mk} + \mathrm{Tr}\{\mathbf{Z}_m\} = 1$ for the optimal solution to Problem $\mathbf{P_{3.3}}$.

Problem $\mathbf{P_{3.3}}$ is still non-convex due to the non-convex constraints (45b), (48a) and (49). Nevertheless, one can find that both sides of (45b), (48a) and (49) are convex functions. Therefore, by their first-order approximations, we can come up with the following restricted convex approximation problem:

$$\mathbf{P_{3.4}}: \max_{\{\eta_m, \mathbf{w}_{mk}, \mathbf{Z}_m\}, \mathbf{u}, \boldsymbol{\xi}, v} f_4\left(\{\mathbf{w}_{mk}\}, \{\mathbf{Z}_m\}, \boldsymbol{\iota}, \boldsymbol{\kappa}, \mathbf{u}\right) - q(1 - v) \tag{52a}$$

$$\text{s.t. } u_k \le \widetilde{C}_k\left(\{\mathbf{w}_{mk}, \bar{\mathbf{w}}_{mk}\}\right), \tag{52b}$$

$$\xi_{mn} \ge \widetilde{D}_{mn}\left(\eta_m, \{\mathbf{w}_{mk}, \bar{\mathbf{w}}_{mk}\}, \mathbf{Z}_m\right), \tag{52c}$$

$$f_1\left(\boldsymbol{\gamma}, \{\mathbf{w}_{mk}\}_k\right) = \sum_{k \in \mathcal{K}} \left(\log_2(1 + \gamma_k) - \frac{\gamma_k}{\ln 2} + \frac{1}{\ln 2} \frac{(1 + \gamma_k) \left| \sum_{m \in \mathcal{M}} \sqrt{p_m} \widehat{\mathbf{h}}_{mk}^H \mathbf{w}_{mk} \right|^2}{A_k\left(\{\mathbf{w}_{mk}, \mathbf{0}\}\right) + \left| \sum_{m \in \mathcal{M}} \sqrt{p_m} \widehat{\mathbf{h}}_{mk}^H \mathbf{w}_{mk} \right|^2} \right) \tag{33}$$

$$f_2\left(\boldsymbol{\gamma}, \{\mathbf{w}_{mk}\}_k, \mathbf{g}\right) = \sum_{k \in \mathcal{K}} \left(\log_2(1 + \gamma_k) - \frac{\gamma_k}{\ln 2} + \frac{2}{\ln 2} \mathrm{Re}\left\{ \sqrt{(1 + \gamma_k)} g_k^* \sum_{m \in \mathcal{M}} \sqrt{p_m} \widehat{\mathbf{h}}_{mk}^H \mathbf{w}_{mk} \right\} \right) - \sum_{k \in \mathcal{K}} \frac{|g_k|^2}{\ln 2} \left(A_k\left(\{\mathbf{w}_{mk}, \mathbf{0}\}\right) + \left| \sum_{m \in \mathcal{M}} \sqrt{p_m} \widehat{\mathbf{h}}_{mk}^H \mathbf{w}_{mk} \right|^2 \right) \tag{35}$$

$$f_3\left(\{\mathbf{w}_{mk}\}, \{\mathbf{Z}_m\}, \boldsymbol{\iota}, \boldsymbol{\kappa}\right) = \sum_{k \in \mathcal{K}} \log_2(1 + \iota_k) + \sum_{k \in \mathcal{K}} \frac{2}{\ln 2} \mathrm{Re}\left\{ \sqrt{(1 + \iota_k)} \kappa_k^* \sum_{m \in \mathcal{M}} \sqrt{p_m} \widehat{\mathbf{h}}_{mk}^H \mathbf{w}_{mk} \right\} - \sum_{k \in \mathcal{K}} \frac{|\kappa_k|^2}{\ln 2} \left(A_k\left(\{\mathbf{w}_{mk}, \mathbf{Z}_m\}\right) + \left| \sum_{m \in \mathcal{M}} \sqrt{p_m} \widehat{\mathbf{h}}_{mk}^H \mathbf{w}_{mk} \right|^2 \right) - \sum_{k \in \mathcal{K}} \frac{\iota_k}{\ln 2} \tag{38}$$

$$\sum_{k\in\mathcal{K}}\left(\bar{\mathbf{w}}_{mk}^H\bar{\mathbf{w}}_{mk}+2\mathrm{Re}\left\{\bar{\mathbf{w}}_{mk}^H\left(\mathbf{w}_{mk}-\bar{\mathbf{w}}_{mk}\right)\right\}\right)+\mathrm{Tr}\left\{\mathbf{Z}_m\right\}\geq v, \tag{52d}$$
$$(14),(24c),(48b),(48c),(50),$$
$$\forall m\in\mathcal{M}_{\mathrm{T}},\forall k\in\mathcal{K},n\in\mathcal{N},$$

where $\{\bar{\mathbf{w}}_{mk}\}$ is feasible to Problem $\mathbf{P_{3.3}}$, and $\widetilde{C}_k\left(\{\mathbf{w}_{mk},\bar{\mathbf{w}}_{mk}\}\right)$ and $\widetilde{D}_{mn}(\eta_m,\{\mathbf{w}_{mk},\bar{\mathbf{w}}_{mk}\},\mathbf{Z}_m)$ are given in (53) and (54), as shown at the bottom of the next page, respectively. Then one can apply the SCA method [49] to Problem $\mathbf{P_{3.4}}$ in order to get a good sub-optimal solution to Problem $\mathbf{P_3}$, thereby yielding the proposed BCD-SCA based algorithm (termed Algorithm 3) for this end.

Algorithm 3 The Proposed BCD-SCA Based Algorithm for Solving Problem $\mathbf{P_3}$

Initialization:
Find a feasible $\{\bar{\mathbf{w}}_{mk},\bar{\mathbf{Z}}_m\}$ to Problem $\mathbf{P_{3.3}}$;
Calculate $\boldsymbol{\iota}$ and $\boldsymbol{\kappa}$ with $\{\bar{\mathbf{w}}_{mk},\bar{\mathbf{Z}}_m\}$ by (39) and (40), respectively;
while *the stop criterion is not satified* **do**
  while *the stop criterion is not satified* **do**
    Obtain the optimal solution $\{\mathbf{w}_{mk}^\star,\mathbf{Z}_m^\star\}$ by solving Problem $\mathbf{P_{3.4}}$ with $\boldsymbol{\iota}$, $\boldsymbol{\kappa}$ and $\{\bar{\mathbf{w}}_{mk}\}$;
    Update $\{\bar{\mathbf{w}}_{mk}\}:=\{\mathbf{w}_{mk}^\star\}$;
  end
  Update $\boldsymbol{\iota}$ with $\{\mathbf{w}_{mk}^\star,\mathbf{Z}_m^\star\}$ by (39);
  Update $\boldsymbol{\kappa}$ with $\{\mathbf{w}_{mk}^\star,\mathbf{Z}_m^\star\}$ and $\boldsymbol{\iota}$ by (40);
end

By solving Problem $\mathbf{P_{3.4}}$ via a standard interior-point method, the computational complexity of Algorithm 3 is

$$\mathcal{O}\left\{I_2\sqrt{3TN+TN_{\mathrm{T}}+2M+K}\psi\left(\psi\left(TN+K+TN_{\mathrm{T}}^2\right)+MK^2N_{\mathrm{T}}^2+TN(KN_{\mathrm{T}}+N_{\mathrm{T}}^2)^2\right)\right\},$$

TABLE I
SYSTEM PARAMETERS USED IN SIMULATION

AP Parameters	Values	IU Parameters	Values
M	6	K	9
N_{T}	12	p_{p}	150 dB
p_m	125 dB	τ_{p}	5
D	2 km	τ_{c}	40
$\sigma^2_{\mathrm{T}_t,\mathrm{A}_m}$	-160 dB	$\sigma^2_{\mathrm{U}_k,\mathrm{T}_t}$	-160 dB
Target Parameters	**Values**	**Target Parameters**	**Values**
T	3	α_t	0.8
$\Delta\theta$	10°	N	181
$\chi^2_{\mathrm{T}_t,\mathrm{A}_m}$	-30 dB	q	1000

where I_2 denotes the number of required iterations to converge for Algorithm 3, and $\psi=MKN_{\mathrm{T}}+TN_{\mathrm{T}}^2+TN+T+K+1$ denotes the decision variable dimension of Problem $\mathbf{P_{3.4}}$.

V. NUMERICAL RESULTS

In this section, some numerical results are presented to show the proposed C-S region of the Cell-Free massive MIMO ISAC system, i.e., the set $\mathcal{R}_{\text{C-S}}$ defined in (21), as well as its characteristics, insights and impacts of system parameters on the C-S performance trade-off. The system parameters used in the obtained numerical results are listed in Table I, provided that all the APs, IUs, and targets are uniformly distributed within a square of $D\times D$ (km^2).

Figure 3(a) shows a 3-dimensional (3)-D) C-S region of the considered Cell-Free massive MIMO ISAC system obtained using all the algorithms proposed in Sections III and IV, where the x-axis, y-axis and z-axis respectively represent the number of APs, sensing performance (in MSE) and communication performance (in sum rate). For fairness, the total number of antennas is fixed as 48 and evenly distributed among APs,[4] i.e.,

[4]A fixed power budget is allocated to each ISAC AP to guarantee its probing range, while the communication-only APs share the remaining available power evenly.

$$B_k\left(\{\mathbf{w}_{mk},\mathbf{Z}_m\}\right)\triangleq\sum_{k'\neq k}\left|\sum_{m\in\mathcal{M}}\sqrt{p_m}\widehat{\mathbf{h}}_{mk}^H\mathbf{w}_{mk'}\right|^2+\sum_{k'\in\mathcal{K}}\sum_{m\in\mathcal{M}}p_m\mathbf{w}_{mk'}^H\boldsymbol{\Theta}_{mk}\mathbf{w}_{mk'}+1+\sum_{m\in\mathcal{M}_{\mathrm{T}}}p_m\left(\widehat{\mathbf{h}}_{mk}^H\mathbf{Z}_m\widehat{\mathbf{h}}_{mk}+\mathrm{Tr}\left\{\boldsymbol{\Theta}_{mk}\mathbf{Z}_m\right\}\right)+\sum_{k'\in\mathcal{K}}\sum_{m\in\mathcal{M}}\sum_{m'>m}\left|\sqrt{p_m}\boldsymbol{\Theta}_{mm'k}^H\mathbf{w}_{mk'}+\sqrt{p_{m'}}\mathbf{w}_{m'k'}\right|^2 \tag{42}$$

$$C_k\left(\{\mathbf{w}_{mk}\}\right)\triangleq\sum_{k'\in\mathcal{K}}\sum_{m\in\mathcal{M}}\sum_{m'>m}\left(p_m\mathbf{w}_{mk'}^H\boldsymbol{\Theta}_{mm'k}\boldsymbol{\Theta}_{mm'k}^H\mathbf{w}_{mk'}+p_{m'}\mathbf{w}_{m'k'}^H\mathbf{w}_{m'k'}\right) \tag{43}$$

$$f_4\left(\{\mathbf{w}_{mk}\},\{\mathbf{Z}_m\},\boldsymbol{\iota},\boldsymbol{\kappa},\mathbf{u}\right)=\sum_{k\in\mathcal{K}}\log_2(1+\iota_k)+\sum_{k\in\mathcal{K}}\frac{2}{\ln 2}\mathrm{Re}\left\{\sqrt{(1+\iota_k)}\kappa_k^*\sum_{m\in\mathcal{M}}\sqrt{p_m}\widehat{\mathbf{h}}_{mk}^H\mathbf{w}_{mk}\right\}-\sum_{k\in\mathcal{K}}\frac{|\kappa_k|^2}{\ln 2}\left(B_k\left(\{\mathbf{w}_{mk},\mathbf{Z}_m\}\right)-u_k+\left|\sum_{m\in\mathcal{M}}\sqrt{p_m}\widehat{\mathbf{h}}_{mk}^H\mathbf{w}_{mk}\right|^2\right)-\sum_{k\in\mathcal{K}}\frac{\iota_k}{\ln 2} \tag{46}$$

$$D_{mn}\left(\eta_m,\{\mathbf{w}_{mk}\},\mathbf{Z}_m\right)\triangleq\eta_m\widetilde{P}_m(\bar{\theta}_n)-p_m\mathbf{a}^H(\bar{\theta}_n)\left(\sum_{k\in\mathcal{K}}\mathbf{w}_{mk}\mathbf{w}_{mk}^H+\mathbf{Z}_m\right)\mathbf{a}(\bar{\theta}_n) \tag{47}$$

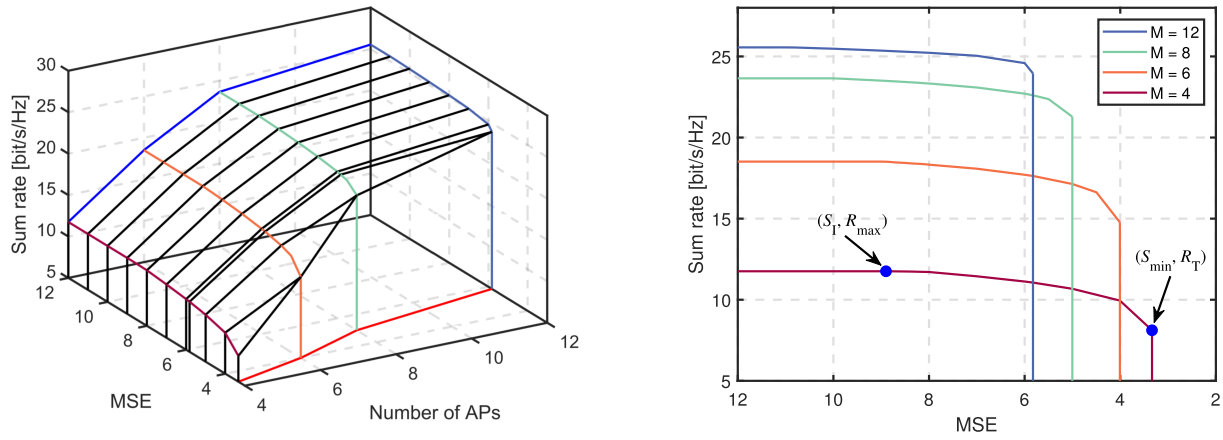

(a) The impact of the APs' number on the C-S region of the ISAC.

(b) C-S region of the ISAC for $M \in \{4, 6, 8, 12\}$.

Fig. 3. The C-S region in Cell-Free massive MIMO ISAC systems.

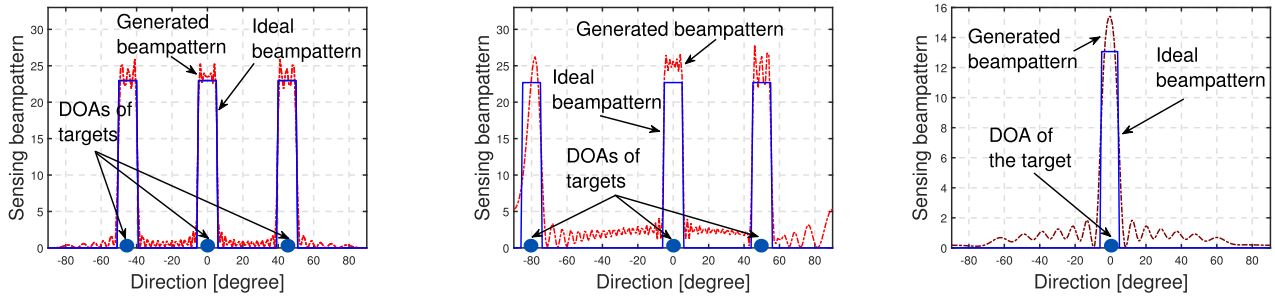

(a) Traditional cellular system with DOAs of targets being $(-45^\circ, 0^\circ, 45^\circ)$.

(b) Traditional cellular system with DOAs of targets being $(-80^\circ, 0^\circ, 50^\circ)$.

(c) Cell-Free system (beampatterns are almost the same for each AP).

Fig. 4. Sensing-only comparison (under 3 targets) between the traditional cellular system (one BS equipped with 48 antennas) and the Cell-Free system (3 APs, each equipped with 16 antennas).

$N_{\mathrm{T}} = 48/M$. One can observe that the sum rate increases with the number of APs (M), because the average distance between each IU and all the APs decreases, namely resulting in smaller path loss between them. In addition, the MSE also increases with M due to smaller N_{T} used for each target sensing (with larger mainlobe width or less focused on the target). Nevertheless, it is by no means that the Cell-Free ISAC is inferior to the traditional ISAC, and more insights are to be discussed in Figure 4 below. Figure 3(b) shows the projection of the 3-D C-S region on the (S, R) plane for $M \in \{4, 6, 8, 12\}$. It is observed that the C-S region with a larger M does not cover the C-S region with a smaller M, and vice versa. Therefore, the trade-off between communication and sensing in the Cell-Free ISAC system can be adjusted by setting the value of M. To derive more insights, we focus on the C-S region with $M = 4$, where the two critical points $(S_{\mathrm{I}}, R_{\max})$ and $(S_{\min}, R_{\mathrm{T}})$ on the boundary of the resulting 2-D C-S region of the ISAC reveal the achievable maximum sum rate $R_{\max}$ and minimum MSE $S_{\min}$, respectively. As stated in Remark 2, the C-S performance trade-off exists only on the boundary between the two critical points, depending on the given finite resource. Note that if $\delta < S_{\min}$ ($\zeta > R_{\max}$) Problem $\mathbf{P_3}$ ($\mathbf{P_4}$) is infeasible.

Let us consider the sensing-only case of $T = 3$ targets for a performance comparison of the traditional system (i.e., one BS equipped with 48 antennas) and the Cell-Free system (with $N_{\mathrm{T}} = 16$ antennas for each of the 3 APs). Figure 4 shows the designed beampatterns for the sensing-only case, for 3 targets with estimated DOA being $(-45^\circ, 0^\circ, 45^\circ)$ in Figure 4(a) and $(-80^\circ, 0^\circ, 50^\circ)$ in Figure 4(b) for the traditional cellular system, while only one target with estimated DOA being 0° in Figure 4(c) for Cell-Free system. For a fair comparison, to take the probing range into account, we consider the normalized MSE instead, which is defined as

$$\widetilde{C}_k\left(\{\mathbf{w}_{mk}, \bar{\mathbf{w}}_{mk}\}\right) \triangleq \sum_{k' \in \mathcal{K}} \sum_{m \in \mathcal{M}} \sum_{m' > m} \left(p_m \bar{\mathbf{w}}_{mk'}^H \boldsymbol{\Theta}_{mm'k} \boldsymbol{\Theta}_{mm'k}^H \bar{\mathbf{w}}_{mk'} + p_{m'} \bar{\mathbf{w}}_{m'k'}^H \bar{\mathbf{w}}_{m'k'} + 2\mathrm{Re}\left\{p_m \bar{\mathbf{w}}_{mk'}^H \boldsymbol{\Theta}_{mm'k} \boldsymbol{\Theta}_{mm'k}^H \left(\mathbf{w}_{mk'} - \bar{\mathbf{w}}_{mk'}\right) + p_{m'} \bar{\mathbf{w}}_{m'k'}^H \left(\mathbf{w}_{m'k'} - \bar{\mathbf{w}}_{m'k'}\right)\right\}\right) \tag{53}$$

$$\widetilde{D}_{mn}\left(\eta_m, \{\mathbf{w}_{mk}, \bar{\mathbf{w}}_{mk}\}, \mathbf{Z}_m\right) \triangleq \eta_m \widetilde{P}_m(\bar{\theta}_n) - p_m \mathbf{a}^H(\bar{\theta}_n) \left(\sum_{k \in \mathcal{K}} \left(\bar{\mathbf{w}}_{mk} \bar{\mathbf{w}}_{mk}^H + 2\mathrm{Re}\left\{\bar{\mathbf{w}}_{mk} (\mathbf{w}_{mk} - \bar{\mathbf{w}}_{mk})^H\right\}\right) + \mathbf{Z}_m\right) \mathbf{a}(\bar{\theta}_n) \tag{54}$$

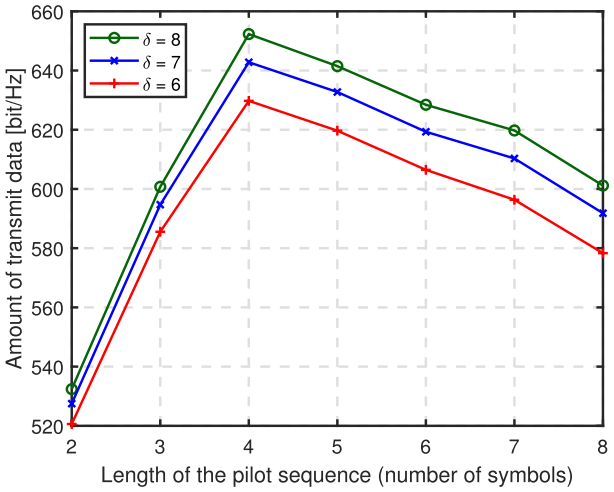

Fig. 5. The amount of transmit data versus the length of the pilot sequence.

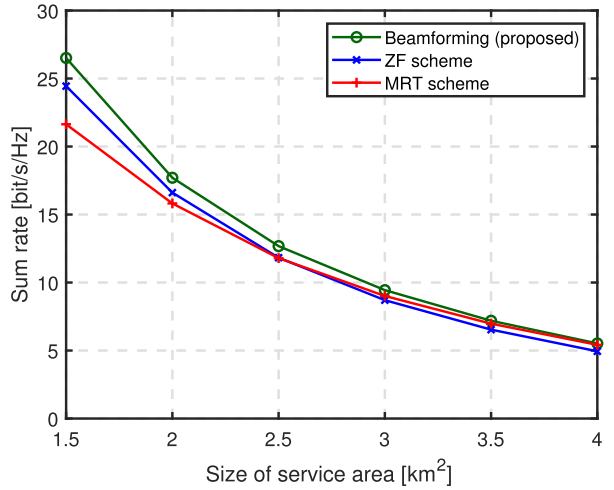

Fig. 6. Comparison among the proposed beamforming scheme, the ZF scheme and the MRT scheme with $\delta = 6$.

$\sum_{m\in\mathcal{M}_{\mathrm{T}}} \mathcal{E}_m\left(\eta_m, \{\mathbf{w}_{mk}\}, \mathbf{Z}_m\right)/(M_{\mathrm{T}}\eta_m^2)$. Over 2000 realizations of the targets' positions, the obtained average normalized MSE of the centralized traditional cellular system is 0.0159, while that of the Cell-Free system is 0.0080 (around half of the former), thereby demonstrating much better performance for the distributed Cell-Free system. Furthermore, it can be seen from Figure 4(a) and Figure 4(b) that the beampattern matching quality is quite sensitive to the dispersiveness of the target distribution for the traditional cellular system, so is its sensing performance. On the contrary, in the Cell-Free system, each AP is dedicated to only one target, thus readily maintaining the target DOA being 0° as shown in Figure 4(c), in other words, the sensing performance of the Cell-Free system is robust against the target distribution.

Figure 5 shows the impact of the length of the pilot sequence, i.e., τ_{p}, on the amount of transmit data, given by $(\tau_{\mathrm{c}}-\tau_{\mathrm{p}})\sum_{k\in\mathcal{K}} r_k(\{\mathbf{w}_{mk}, \mathbf{Z}_m\})$. It can be observed that the amount of transmit data first increases, reaches the maximum for $\tau_{\mathrm{p}} = 4$, and then decreases with τ_{p}. The reason is because a larger τ_{p} can bring a smaller channel estimation error (thus improving the downlink transmission rate) but a shorter downlink transmission time, i.e., $(\tau_{\mathrm{c}}-\tau_{\mathrm{p}})$, thus making the amount of transmit data decrease for $\tau_{\mathrm{p}} > 4$ instead. Moreover, the larger the δ (i.e., lower sensing beampattern matching MSE requirement), the larger the power allocated to downlink transmission, thereby yielding more data transmitted.

Figure 6 shows the sum rate performance of the proposed beamforming of ISAC with $\delta = 6$ (implemented by Algorithm 3), and a comparison with the ZF scheme and the MRT scheme for different sizes of service area of the considered system. One can see from this figure that all the 3 schemes' performances are worse for larger service area, simply because of larger average path loss incurred. Nonetheless, the proposed scheme outperforms the other two schemes, and the ZF scheme performs better (worse) than the MRT scheme for relatively smaller (larger) service area, which is consistent with the results reported in [50], as larger area corresponds to smaller SNR under the constraint on fixed power budget.

VI. Conclusion

We have presented a novel system model and a downlink transmit beamforming design for the Cell-Free massive MIMO ISAC system, based on the first-order and second-order statistics of the MIMO channel estimation error (via the uplink pilot training) that were theoretically obtained for the first time to the best of our knowledge. The achievable C-S region of the ISAC system under constraints of finite resources, has also been presented that can be obtained via beamforming designs for 3 cases (sensing-only case, communication-only case and ISAC case) using the proposed algorithms in Section III and IV. Then some numerical results were provided to demonstrate the obtained C-S region and its various characteristics, specifically, the performance trade-off between communication and radar sensing on the boundary of the C-S region, the impacts of the system parameters on the beamforming performance, and advantages of the proposed beamformer beyond those used in state-of-the-art ISAC systems. Some further studies, including i) C-S performance trade-off sensitivity to various system parameters, ii) each AP sensing multiple targets, and iii) incorporation of target detection performance, are left in the future.

Appendix A
Proof of Proposition 1

For the aggregated channel, the direct link and the cascade links are statistically independent, so are the cascade links reflected from different targets. Then, the auto-correlation matrix of $\mathbf{h}_{mk}$, the cross-correlation matrix of $\mathbf{h}_{mk}$ and $\mathbf{h}_{m'k}$ $(m' \neq m)$, and the cross-correlation matrix of $\mathbf{h}_{mk}$ and $\mathbf{h}_{mk'}$ $(k' \neq k)$ are respectively given by

$$\begin{aligned}
&\mathbb{E}\left\{\mathbf{h}_{mk}\mathbf{h}_{mk}^H\right\} \\
&= \mathbb{E}\left\{\mathbf{h}_{\mathrm{U}_k,\mathrm{A}_m}\mathbf{h}_{\mathrm{U}_k,\mathrm{A}_m}^H\right\} \\
&\quad + \sum_{t\in\mathcal{T}} \alpha_t^2 \mathbb{E}\left\{|h_{\mathrm{U}_k,\mathrm{T}_t}|^2\right\}\mathbb{E}\left\{\mathbf{h}_{\mathrm{T}_t,\mathrm{A}_m}\mathbf{h}_{\mathrm{T}_t,\mathrm{A}_m}^H\right\}, \\
&\mathbb{E}\left\{\mathbf{h}_{mk}\mathbf{h}_{m'k}^H\right\} \\
&= \mathbb{E}\left\{\mathbf{h}_{\mathrm{U}_k,\mathrm{A}_m}\mathbf{h}_{\mathrm{U}_k,\mathrm{A}_{m'}}^H\right\}
\end{aligned}$$

$$+\sum_{t\in\mathcal{T}}\alpha_t^2\mathbb{E}\left\{|h_{\mathrm{U}_k,\mathrm{T}_t}|^2\right\}\mathbb{E}\left\{\mathbf{h}_{\mathrm{T}_t,\mathrm{A}_m}\mathbf{h}_{\mathrm{T}_t,\mathrm{A}_{m'}}^H\right\},$$

and $\mathbb{E}\left\{\mathbf{h}_{mk}\mathbf{h}_{mk'}^H\right\}$

$$=\mathbb{E}\left\{\mathbf{h}_{\mathrm{U}_k,\mathrm{A}_m}\mathbf{h}_{\mathrm{U}_{k'},\mathrm{A}_m}^H\right\}+\sum_{t\in\mathcal{T}}\alpha_t^2\mathbb{E}\left\{h_{\mathrm{U}_k,\mathrm{T}_t}h_{\mathrm{U}_{k'},\mathrm{T}_t}^*\right\}\mathbb{E}\left\{\mathbf{h}_{\mathrm{T}_t,\mathrm{A}_m}\mathbf{h}_{\mathrm{T}_t,\mathrm{A}_m}^H\right\}.$$

According to the corresponding channel models in Section II-A, it holds that $\mathbb{E}\{\mathbf{h}_{\mathrm{U}_k,\mathrm{A}_m}\}=\mathbf{0}$, $\mathbb{E}\{\mathbf{h}_{\mathrm{U}_k,\mathrm{A}_m}\mathbf{h}_{\mathrm{U}_k,\mathrm{A}_m}^H\}=\beta^2(d_{\mathrm{U}_k,\mathrm{A}_m})\mathbf{I}_{N_\mathrm{T}}$, $\mathbb{E}\{h_{\mathrm{U}_k,\mathrm{T}_t}\}=0$, $\mathbb{E}\{|h_{\mathrm{U}_k,\mathrm{T}_t}|^2\}=\beta^2(\bar{d}_{\mathrm{U}_k,\mathrm{T}_t})+\sigma_{\mathrm{U}_k,\mathrm{T}_t}^2$, $\mathbb{E}\{\mathbf{h}_{\mathrm{T}_t,\mathrm{A}_m}\}=\beta(\bar{d}_{\mathrm{T}_t,\mathrm{A}_m})\bar{\mathbf{q}}_{\mathrm{T}_t,\mathrm{A}_m}$ and $\mathbb{E}\{\mathbf{h}_{\mathrm{T}_t,\mathrm{A}_m}\mathbf{h}_{\mathrm{T}_t,\mathrm{A}_m}^H\}=(\beta^2(\bar{d}_{\mathrm{T}_t,\mathrm{A}_m})+\sigma_{\mathrm{T}_t,\mathrm{A}_m}^2)(\bar{\mathbf{q}}_{\mathrm{T}_t,\mathrm{A}_m}\bar{\mathbf{q}}_{\mathrm{T}_t,\mathrm{A}_m}^H+\chi_{\mathrm{T}_t,\mathrm{A}_m}^2\mathbf{I}_{N_\mathrm{T}})$. Then, one can find that $\mathbb{E}\{\mathbf{h}_{mk}\mathbf{h}_{mk}^H\}=\mathbf{\Phi}_{mk}$ and $\mathbb{E}\{\mathbf{h}_{mk}\mathbf{h}_{m'k}^H\}=\mathbf{\Phi}_{mm'k}$. Besides, due to both $\{\mathbf{h}_{\mathrm{U}_k,\mathrm{A}_m}\}$ and $\{h_{\mathrm{U}_k,\mathrm{T}_t}\}$ are zero-mean and statistically independent, $\mathbb{E}\{\mathbf{h}_{mk}\mathbf{h}_{mk'}^H\}=\mathbf{0}$. Similarly, $\mathbb{E}\{\mathbf{h}_{mk}\mathbf{h}_{m'k'}^H\}=\mathbf{0}$ $(m'\neq m,k'\neq k)$ can be proved.

APPENDIX B
PROOF OF PROPOSITION 2

According to the definition of $\mathbf{C}_{mk}$ in (10), it holds that

$$\begin{aligned}\mathbb{E}\left\{\widehat{\mathbf{h}}_{mk}\right\}&=\mathbf{C}_{mk}\mathbb{E}\left\{\mathbf{y}_{\mathrm{p},mk}\right\}=\mathbf{0}\text{ and}\\ \mathbb{E}\left\{\widehat{\mathbf{h}}_{mk}\widehat{\mathbf{h}}_{mk}^H\right\}&=\mathbf{C}_{mk}\mathbb{E}\left\{\mathbf{y}_{\mathrm{p},mk}\mathbf{y}_{\mathrm{p},mk}^H\right\}\mathbf{C}_{mk}^H\\&=\mathbf{C}_{mk}\mathbb{E}\left\{\mathbf{y}_{\mathrm{p},mk}\mathbf{h}_{mk}^H\right\}\\&=\sqrt{p_\mathrm{p}\tau_\mathrm{p}}\mathbf{C}_{mk}\mathbb{E}\left\{\mathbf{h}_{mk}\mathbf{h}_{mk}^H\right\}\\&=\sqrt{p_\mathrm{p}\tau_\mathrm{p}}\mathbf{C}_{mk}\mathbf{\Phi}_{mk}.\end{aligned}$$

That is, the derivation of $\mathbb{E}\{\widehat{\mathbf{h}}_{mk}\widehat{\mathbf{h}}_{mk}^H\}$ is equivalent to the computation of $\mathbf{C}_{mk}$ which includes two parts, i.e., $\mathbb{E}\{\mathbf{h}_{mk}\mathbf{y}_{\mathrm{p},mk}^H\}$ and $\mathbb{E}\{\mathbf{y}_{\mathrm{p},mk}\mathbf{y}_{\mathrm{p},mk}^H\}$. The former can be obtained by

$$\begin{aligned}\mathbb{E}\left\{\mathbf{h}_{mk}\mathbf{y}_{\mathrm{p},mk}^H\right\}&=\sqrt{p_\mathrm{p}\tau_\mathrm{p}}\mathbb{E}\left\{\mathbf{h}_{mk}\mathbf{h}_{mk}^H\right\}+\mathbb{E}\left\{\mathbf{h}_{mk}\mathbf{n}_{\mathrm{p},mk}^H\right\}\\&\quad+\sqrt{p_\mathrm{p}\tau_\mathrm{p}}\sum_{k'\in\mathcal{P}_k\setminus\{k\}}\mathbb{E}\left\{\mathbf{h}_{mk}\mathbf{h}_{mk'}^H\right\}\\&=\sqrt{p_\mathrm{p}\tau_\mathrm{p}}\mathbf{\Phi}_{mk},\end{aligned}$$

and the latter as

$$\begin{aligned}\mathbb{E}\{\mathbf{y}_{\mathrm{p},mk}\mathbf{y}_{\mathrm{p},mk}^H\}&=p_\mathrm{p}\tau_\mathrm{p}\sum_{k'\in\mathcal{P}_k}\mathbb{E}\left\{\mathbf{h}_{mk'}\mathbf{h}_{mk'}^H\right\}+\mathbf{I}_{N_\mathrm{T}}\\&=p_\mathrm{p}\tau_\mathrm{p}\sum_{k'\in\mathcal{P}_k}\mathbf{\Phi}_{mk'}+\mathbf{I}_{N_\mathrm{T}}.\end{aligned}$$

Therefore, the closed-form expression of $\mathbf{C}_{mk}$ is given by

$$\mathbf{C}_{mk}=\sqrt{p_\mathrm{p}\tau_\mathrm{p}}\mathbf{\Phi}_{mk}\left(p_\mathrm{p}\tau_\mathrm{p}\sum_{k'\in\mathcal{P}_k}\mathbf{\Phi}_{mk'}+\mathbf{I}_{N_\mathrm{T}}\right)^{-1}.$$

APPENDIX C
PROOF OF PROPOSITION 3

For the channel estimation error $\mathbf{e}_{mk}$ defined by (11), it holds that

$$\mathbb{E}\left\{\mathbf{e}_{mk}\right\}=\mathbb{E}\left\{\mathbf{h}_{mk}\right\}-\mathbb{E}\left\{\widehat{\mathbf{h}}_{mk}\right\}=\mathbf{0}.$$

According to properties of linear MMSE method [38], the channel estimation error $\mathbf{e}_{mk}$ and the channel estimation $\widehat{\mathbf{h}}_{mk}$ are orthogonal. Thus, the auto-correlation matrix of $\mathbf{e}_{mk}$ is given by

$$\begin{aligned}\mathbb{E}\left\{\mathbf{e}_{mk}\mathbf{e}_{mk}^H\right\}&=\mathbb{E}\left\{\left(\mathbf{h}_{mk}-\widehat{\mathbf{h}}_{mk}\right)\left(\mathbf{h}_{mk}-\widehat{\mathbf{h}}_{mk}\right)^H\right\}\\&=\mathbb{E}\{\mathbf{h}_{mk}\mathbf{h}_{mk}^H\}-\mathbb{E}\{\widehat{\mathbf{h}}_{mk}\widehat{\mathbf{h}}_{mk}^H\}\\&=\mathbf{\Phi}_{mk}-\sqrt{p_\mathrm{p}\tau_\mathrm{p}}\mathbf{C}_{mk}\mathbf{\Phi}_{mk}=\mathbf{\Theta}_{mk},\end{aligned}$$

and the cross-correlation matrix of $\mathbf{e}_{mk}$ and $\mathbf{e}_{m'k}$ $(m'\neq m)$ is given by

$$\begin{aligned}&\mathbb{E}\left\{\mathbf{e}_{mk}\mathbf{e}_{m'k}^H\right\}\\&=\mathbb{E}\left\{\mathbf{h}_{mk}\mathbf{h}_{m'k}^H\right\}+\mathbb{E}\left\{\mathbf{C}_{mk}\mathbf{y}_{\mathrm{p},mk}\mathbf{y}_{\mathrm{p},m'k}^H\mathbf{C}_{m'k}^H\right\}\\&\quad-\mathbb{E}\left\{\mathbf{h}_{mk}\mathbf{y}_{\mathrm{p},m'k}^H\mathbf{C}_{m'k}^H\right\}-\mathbb{E}\left\{\mathbf{C}_{mk}\mathbf{y}_{\mathrm{p},mk}\mathbf{h}_{m'k}^H\right\}\\&=\mathbf{\Phi}_{mm'k}+p_\mathrm{p}\tau_\mathrm{p}\mathbf{C}_{mk}\sum_{k'\in\mathcal{P}_k}\mathbf{\Phi}_{mm'k'}\mathbf{C}_{m'k}^H\\&\quad-\sqrt{p_\mathrm{p}\tau_\mathrm{p}}\mathbf{\Phi}_{mm'k}\mathbf{C}_{m'k}^H-\sqrt{p_\mathrm{p}\tau_\mathrm{p}}\mathbf{C}_{mk}\mathbf{\Phi}_{mm'k}=\mathbf{\Theta}_{mm'k}.\end{aligned}$$

REFERENCES

[1] D. Xu, X. Yu, D. W. K. Ng, A. Schmeink, and R. Schober, "Robust and secure resource allocation for ISAC systems: A novel optimization framework for variable-length snapshots," *IEEE Trans. Commun.*, vol. 70, no. 12, pp. 8196–8214, Dec. 2022.

[2] B. Li, Y. Liu, L. Tan, H. Pan, and Y. Zhang, "Digital twin assisted task offloading for aerial edge computing and networks," *IEEE Trans. Veh. Technol.*, vol. 71, no. 10, pp. 10863–10877, Oct. 2022.

[3] W. Mao, K. Xiong, Y. Lu, P. Fan, and Z. Ding, "Energy consumption minimization in secure multi-antenna UAV-assisted MEC networks with channel uncertainty," *IEEE Trans. Wireless Commun.*, vol. 22, no. 11, pp. 7185–7200, Nov. 2023.

[4] W. Liu, B. Li, W. Xie, Y. Dai, and Z. Fei, "Energy efficient computation offloading in aerial edge networks with multi-agent cooperation," *IEEE Trans. Wireless Commun.*, vol. 22, no. 9, pp. 5725–5739, Sep. 2023.

[5] R. Yang, C.-X. Wang, J. Huang, E.-H. M. Aggoune, and Y. Hao, "A novel 6G ISAC channel model combining forward and backward scattering," *IEEE Trans. Wireless Commun.*, vol. 22, no. 11, pp. 8050–8065, Nov. 2023, doi: 10.1109/TWC.2023.3258150.

[6] L. Zheng, M. Lops, and X. Wang, "Adaptive interference removal for uncoordinated radar/communication coexistence," *IEEE J. Sel. Topics Signal Process.*, vol. 12, no. 1, pp. 45–60, Feb. 2018.

[7] T. Huang, N. Shlezinger, X. Xu, Y. Liu, and Y. C. Eldar, "MAJoRCom: A dual-function radar communication system using index modulation," *IEEE Trans. Signal Process.*, vol. 68, pp. 3423–3438, 2020.

[8] D. Ma et al., "Spatial modulation for joint radar-communications systems: Design, analysis, and hardware prototype," *IEEE Trans. Veh. Technol.*, vol. 70, no. 3, pp. 2283–2298, Mar. 2021.

[9] T. Choi et al., "Experimental investigation of frequency domain channel extrapolation in massive MIMO systems for zero-feedback FDD," *IEEE Trans. Wireless Commun.*, vol. 20, no. 1, pp. 710–725, Jan. 2021.

[10] H. Q. Ngo, A. Ashikhmin, H. Yang, E. G. Larsson, and T. L. Marzetta, "Cell-free massive MIMO versus small cells," *IEEE Trans. Wireless Commun.*, vol. 16, no. 3, pp. 1834–1850, Mar. 2017.

[11] Y. Fang, L. Qiu, X. Liang, and C. Ren, "Cell-free massive MIMO systems with oscillator phase noise: Performance analysis and power control," *IEEE Trans. Veh. Technol.*, vol. 70, no. 10, pp. 10048–10064, Oct. 2021.

[12] F. Liu et al., "Integrated sensing and communications: Toward dual-functional wireless networks for 6G and beyond," *IEEE J. Sel. Areas Commun.*, vol. 40, no. 6, pp. 1728–1767, Jun. 2022.

[13] R. Liu, M. Li, Y. Liu, Q. Wu, and Q. Liu, "Joint transmit waveform and passive beamforming design for RIS-aided DFRC systems," *IEEE J. Sel. Topics Signal Process.*, vol. 16, no. 5, pp. 995–1010, Aug. 2022.

[14] D. Xu, A. Khalili, X. Yu, D. Wing Kwan Ng, and R. Schober, "Integrated sensing and communication in distributed antenna networks," in *Proc. IEEE Int. Conf. Commun. Workshops*, Jun. 2023, pp. 1457–1462.

[15] F. Wang and H. Li, "Power allocation for coexisting multicarrier radar and communication systems in cluttered environments," *IEEE Trans. Signal Process.*, vol. 69, pp. 1603–1613, 2021.

[16] Y. He, Y. Cai, H. Mao, and G. Yu, "RIS-assisted communication radar coexistence: Joint beamforming design and analysis," *IEEE J. Sel. Areas Commun.*, vol. 40, no. 7, pp. 2131–2145, Jul. 2022.

[17] Z. Cheng and B. Liao, "QoS-aware hybrid beamforming and DOA estimation in multi-carrier dual-function radar-communication systems," *IEEE J. Sel. Areas Commun.*, vol. 40, no. 6, pp. 1890–1905, Jun. 2022.

[18] X. Wang, Z. Fei, J. A. Zhang, and J. Xu, "Partially-connected hybrid beamforming design for integrated sensing and communication systems," *IEEE Trans. Commun.*, vol. 70, no. 10, pp. 6648–6660, Oct. 2022.

[19] D. Xu, C. Liu, S. Song, and D. W. Kwan Ng, "Integrated sensing and communication in coordinated cellular networks," in *Proc. IEEE Stat. Signal Process. Workshop*, Jul. 2023, pp. 90–94.

[20] Z. Xing, R. Wang, and X. Yuan, "Joint active and passive beamforming design for reconfigurable intelligent surface enabled integrated sensing and communication," *IEEE Trans. Commun.*, vol. 71, no. 4, pp. 2457–2474, Apr. 2023, doi: 10.1109/TCOMM.2023.3244246.

[21] Z. Yang, D. Li, N. Zhao, Z. Wu, Y. Li, and D. Niyato, "Secure precoding optimization for NOMA-aided integrated sensing and communication," *IEEE Trans. Commun.*, vol. 70, no. 12, Dec. 2022.

[22] L. Chen, Z. Wang, Y. Du, Y. Chen, and F. R. Yu, "Generalized transceiver beamforming for DFRC with MIMO radar and MU-MIMO communication," *IEEE J. Sel. Areas Commun.*, vol. 40, no. 6, pp. 1795–1808, Jun. 2022.

[23] P. Gao, L. Lian, and J. Yu, "Cooperative ISAC with direct localization and rate-splitting multiple access communication: A Pareto optimization framework," *IEEE J. Sel. Areas Commun.*, vol. 41, no. 5, pp. 1496–1515, May 2023.

[24] Z. Chen and E. Björnson, "Channel hardening and favorable propagation in cell-free massive MIMO with stochastic geometry," *IEEE Trans. Commun.*, vol. 66, no. 11, pp. 5205–5219, Nov. 2018.

[25] H. Song, T. Goldstein, X. You, C. Zhang, O. Tirkkonen, and C. Studer, "Joint channel estimation and data detection in cell-free massive MU-MIMO systems," *IEEE Trans. Wireless Commun.*, vol. 21, no. 6, pp. 4068–4084, Jun. 2022.

[26] T. Van Chien, H. Q. Ngo, S. Chatzinotas, M. Di Renzo, and B. Ottersten, "Reconfigurable intelligent surface-assisted cell-free massive MIMO systems over spatially-correlated channels," *IEEE Trans. Wireless Commun.*, vol. 21, no. 7, pp. 5106–5128, Jul. 2022.

[27] T. C. Mai, H. Q. Ngo, and L.-N. Tran, "Energy efficiency maximization in large-scale cell-free massive MIMO: A projected gradient approach," *IEEE Trans. Wireless Commun.*, vol. 21, no. 8, pp. 6357–6371, Aug. 2022.

[28] J. Zheng, J. Zhang, J. Cheng, V. C. M. Leung, D. W. K. Ng, and B. Ai, "Asynchronous cell-free massive MIMO with rate-splitting," *IEEE J. Sel. Areas Commun.*, vol. 41, no. 5, pp. 1366–1382, May 2023.

[29] P. Liu, K. Luo, D. Chen, and T. Jiang, "Spectral efficiency analysis of cell-free massive MIMO systems with zero-forcing detector," *IEEE Trans. Wireless Commun.*, vol. 19, no. 2, pp. 795–807, Feb. 2020.

[30] Y. Cao and Q.-Y. Yu, "Design and performance analyses of V-OFDM integrated signal for cell-free massive MIMO joint communication and radar system," *IEEE Syst. J.*, vol. 17, no. 4, pp. 5943–5954, Dec. 2023.

[31] Z. Behdad, Ö. T. Demir, K. W. Sung, E. Björnson, and C. Cavdar, "Power allocation for joint communication and sensing in Cell-Free massive MIMO," in *Proc. IEEE GLOBECOM*, Dec. 2022, pp. 4081–4086.

[32] B. Wang, L. Xu, Z. Cheng, and Z. He, "Semi-distributed hybrid beamforming design for cooperative cell-free dual-function radar-communication networks," in *Proc. IEEE ICASSPW*, Jun. 2023, pp. 1–5.

[33] A. Sakhnini, A. Bourdoux, M. Guenach, H. Sahli, and S. Pollin, "Uplink payload power control in cell-free communication and radar networks," in *Proc. GLOBECOM IEEE Global Commun. Conf.*, Dec. 2022, pp. 5111–5116.

[34] R. Zhang, K. Xiong, Y. Lu, B. Gao, P. Fan, and K. B. Letaief, "Joint coordinated beamforming and power splitting ratio optimization in MU-MISO SWIPT-enabled HetNets: A multi-agent DDQN-based approach," *IEEE J. Sel. Areas Commun.*, vol. 40, no. 2, pp. 677–693, Feb. 2022.

[35] J. Li and P. Stoica, *MIMO Radar Signal Processing*. Hoboken, NJ, USA: Wiley, 2008.

[36] J. Wu, W. Yuan, and L. Hanzo, "When UAVs meet ISAC: Real-time trajectory design for secure communications," *IEEE Trans. Veh. Technol.*, vol. 72, no. 12, pp. 16766–16771, Dec. 2023.

[37] K. Meng et al., "Throughput maximization for UAV-enabled integrated periodic sensing and communication," *IEEE Trans. Wireless Commun.*, vol. 22, no. 1, pp. 671–687, Jan. 2023.

[38] S. M. Kay, *Fundamentals of Statistical Signal Processing*. Upper Saddle River, NJ, USA: Prentice-Hall, 1993.

[39] C. Pan, H. Ren, M. Elkashlan, A. Nallanathan, and L. Hanzo, "Weighted sum-rate maximization for the ultra-dense user-centric TDD C-RAN downlink relying on imperfect CSI," *IEEE Trans. Wireless Commun.*, vol. 18, no. 2, pp. 1182–1198, Feb. 2019.

[40] C. Ding, J.-B. Wang, H. Zhang, M. Lin, and G. Y. Li, "Joint MIMO precoding and computation resource allocation for dual-function radar and communication systems with mobile edge computing," *IEEE J. Sel. Areas Commun.*, vol. 40, no. 7, pp. 2085–2102, Jul. 2022.

[41] N. Su, F. Liu, and C. Masouros, "Secure radar-communication systems with malicious targets: Integrating radar, communications and jamming functionalities," *IEEE Trans. Wireless Commun.*, vol. 20, no. 1, pp. 83–95, Jan. 2021.

[42] W. Mao, K. Xiong, Y. Lu, J. You, B. Ai, and Z. Ding, "Transmission design of active RIS-assisted integrated sensing and communication systems," in *Proc. IEEE ICC*, May 2023, pp. 4230–4235.

[43] W. Mao, Y. Lu, J. Liu, B. Ai, Z. Zhong, and Z. Ding, "Beamforming design in cell-free massive MIMO integrated sensing and communication systems," in *Proc. IEEE GLOBECOM*, Dec. 2023, pp. 546–551.

[44] S. Al-Dabooni and D. Wunsch, "Model order reduction based on agglomerative hierarchical clustering," *IEEE Trans. Neural Netw. Learn. Syst.*, vol. 30, no. 6, pp. 1881–1895, Jun. 2019.

[45] D. P. Bertsekas, "A new algorithm for the assignment problem," *Math. Program.*, vol. 21, no. 1, pp. 152–171, Dec. 1981.

[46] X. Ma, Y. Fang, H. Zhang, S. Guo, and D. Yuan, "Cooperative beamforming design for multiple RIS-assisted communication systems," *IEEE Trans. Wireless Commun.*, vol. 21, no. 12, pp. 10949–10963, Dec. 2022.

[47] K. Shen and W. Yu, "Fractional programming for communication systems—Part I: Power control and beamforming," *IEEE Trans. Signal Process.*, vol. 66, no. 10, pp. 2616–2630, May 2018.

[48] K. Shen and W. Yu, "Fractional programming for communication systems—Part II: Uplink scheduling via matching," *IEEE Trans. Signal Process.*, vol. 66, no. 10, pp. 2631–2644, May 2018.

[49] C.-Y. Chi, W.-C. Li, and C.-H. Lin, *Convex Optimization for Signal Processing and Communications: From Fundamentals to Applications*. Boca Raton, FL, USA: CRC Press, Feb. 2017.

[50] L. Wei, C. Huang, G. C. Alexandropoulos, C. Yuen, Z. Zhang, and M. Debbah, "Channel estimation for RIS-empowered multi-user MISO wireless communications," *IEEE Trans. Commun.*, vol. 69, no. 6, pp. 4144–4157, Jun. 2021.

Weihao Mao (Student Member, IEEE) received the bachelor's degree in information and computing science from Beijing Jiaotong University (BJTU), Beijing, China, in 2021, where he is currently pursuing the Ph.D. degree with the School of Computer Science and Technology. His research interests include convex optimization for wireless communications, UAV communications, integrated sensing and communication, and machine learning methods.

Yang Lu (Member, IEEE) received the B.E. and Ph.D. degrees from Beijing Jiaotong University (BJTU), Beijing, China, in 2014 and 2020, respectively. Since 2020, he has been with BJTU, as a Professor of computer and information technology. His current research interests include the convex optimization and machine learning technologies for wireless communications.

Chong-Yung Chi (Life Fellow, IEEE) received the B.S. degree from Tatung Institute of Technology, Taipei, Taiwan, in 1975, the M.S. degree from National Taiwan University, Taipei, in 1977, and the Ph.D. degree from the University of Southern California, Los Angeles, CA, USA, in 1983, all in electrical engineering.

He is currently a Professor with National Tsing Hua University, Hsinchu, Taiwan. He has published more than 240 technical articles (with citations more than 7500 times by Google-Scholar), including more than 90 journal articles (mostly in IEEE TRANSACTIONS ON SIGNAL PROCESSING), more than 140 peer-reviewed conference papers, three book chapters, and two books, including a textbook, *Convex Optimization for Signal Processing and Communications: From Fundamentals to Applications*, CRC Press, 2017 (which has been popularly used in a series of invited intensive short courses at ten top-ranking universities in Mainland China, since 2010 before its publication). His current research interests include signal processing for wireless communications, convex analysis and optimization for blind source separation, biomedical and hyperspectral image analysis, graph based learning and signal processing, and data security and privacy protection in machine learning.

Dr. Chi was a member of the Signal Processing Theory and Methods Technical Committee (SPTM-TC) (2005–2010), the Signal Processing for Communications and Networking Technical Committee (SPCOM-TC) (2011–2016), the Sensor Array and Multichannel Technical Committee (SAM-TC) (2013–2018), and the IEEE Signal Processing Society. He has been a technical program committee member of many IEEE sponsored and cosponsored workshops, symposiums, and conferences on signal processing and wireless communications, including the Co-Organizer and the General Co-Chair of the 2001 IEEE Workshop on Signal Processing Advances in Wireless Communications (SPAWC). He received the 2018 IEEE Signal Processing Society Best Paper Award, entitled "Outage Constrained Robust Transmit Optimization for Multiuser MISO Downlinks: Tractable Approximations by Conic Optimization," IEEE TRANSACTIONS ON SIGNAL PROCESSING, vol. 62, no. 21, November 2014. He was an Associate Editor (AE) of four IEEE journals, including IEEE TRANSACTIONS ON SIGNAL PROCESSING for nine years (May/2001–April/2006, January/2012–December/2015).

Bo Ai (Fellow, IEEE) received the M.S. and Ph.D. degrees from Xidian University, Xi'an, China, in 2002 and 2004, respectively.

He was with Tsinghua University, Beijing, China, where he was an Excellent Postdoctoral Research Fellow, in 2007. He is currently a Professor and an Advisor of Ph.D. candidates with Beijing Jiaotong University, Beijing, where he is also the Deputy Director of the State Key Laboratory of Rail Traffic Control and Safety. He is with the Engineering College, Armed Police Force, Xi'an. He has authored or coauthored six books and 270 scientific research articles and holds 26 invention patents in his research areas. His research interests include the research and applications of orthogonal frequency-division multiplexing techniques, high-power amplifier linearization techniques, radio propagation and channel modeling, global systems for mobile communications for railway systems, and long-term evolution for railway systems. He is a fellow of The Institution of Engineering and Technology. He received many awards, such as the Qiushi Outstanding Youth Award by Hong Kong Qiushi Foundation, the New Century Talents by Chinese Ministry of Education, the Zhan Tianyou Railway Science and Technology Award by Chinese Ministry of Railways, and the Science and Technology New Star by Beijing Municipal Science and Technology Commission. He was the Co-Chair or the Session/Track Chair for many international conferences, such as the 9th International Heavy Haul Conference (2009); the 2011 IEEE International Conference on Intelligent Rail Transportation; HSRCom2011; the 2012 IEEE International Symposium on Consumer Electronics; the 2013 International Conference on Wireless, Mobile and Multimedia; the IEEE Green HetNet 2013; and the IEEE 78th Vehicular Technology Conference (2014). He is an Associate Editor of IEEE TRANSACTIONS ON CONSUMER ELECTRONICS and an Editorial Committee Member of the *Wireless Personal Communications*.

Zhangdui Zhong (Fellow, IEEE) received the B.E. and M.S. degrees from Beijing Jiaotong University, Beijing, China, in 1983 and 1988, respectively.

He is currently a Professor and an Advisor of Ph.D. candidates with Beijing Jiaotong University, Beijing, China. He is also the Director of the School of Computer and Information Technology and the Chief Scientist of the State Key Laboratory of Rail Traffic Control and Safety, Beijing Jiaotong University. He is the Director of the Innovative Research Team of Ministry of Education, Beijing, and the Chief Scientist of Ministry of Railways, Beijing. His research interests include wireless communications for railways, control theory and techniques for railways, and GSM-R systems. His research has been widely used in railway engineering, such as Qinghai-Xizang Railway, Datong-Qinhuangdao Heavy Haul Railway, and many high-speed railway lines in China. He has authored or coauthored seven books, five invention patents, and over 200 scientific research articles in his research area. He is an Executive Council Member of the Radio Association of China, Beijing, and the Deputy Director of the Radio Association, Beijing. He received the MaoYiSheng Scientific Award of China, the ZhanTianYou Railway Honorary Award of China, and the Top Ten Science/Technology Achievements Award of Chinese Universities.

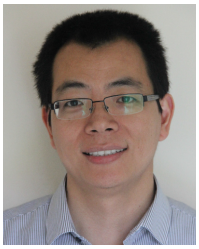

Zhiguo Ding (Fellow, IEEE) received the B.Eng. degree from Beijing University of Posts and Telecommunications in 2000 and the Ph.D. degree from Imperial College London in 2005.

He is currently a Professor of communications with Khalifa University and also affiliated with The University of Manchester and Princeton University. His research interests include B5G networks, energy harvesting networks, and statistical signal processing. He recently received the EU Marie Curie Fellowship 2012–2014, the Top IEEE TVT Editor 2017, the IEEE Heinrich Hertz Award 2018, the IEEE Jack Neubauer Memorial Award 2018, the IEEE Best Signal Processing Letter Award 2018, the Friedrich Wilhelm Bessel Research Award 2020, and the IEEE SPCC Technical Recognition Award 2021. He is a Distinguished Lecturer of IEEE ComSoc and a Web of Science Highly Cited Researcher in two categories in 2022. He was an Editor of IEEE WIRELESS COMMUNICATIONS LETTERS, IEEE TRANSACTIONS ON COMMUNICATIONS, IEEE COMMUNICATIONS LETTERS from 2013 to 2016. He is serving as an Area Editor for the IEEE OPEN JOURNAL OF THE COMMUNICATIONS SOCIETY and an Editor for IEEE TRANSACTIONS ON VEHICULAR TECHNOLOGY and IEEE TRANSACTIONS ON WIRELESS COMMUNICATIONS.